Redox Biology 76 (2024) 103349

Contents lists available at ScienceDirect

Redox Biology

journal homepage: www.elsevier.com/locate/redox

UBR5 mediates colorectal cancer chemoresistance by attenuating ferroptosis via Lys 11 ubiquitin-dependent stabilization of Smad3-SLC7A11 signaling

Mei Song [a,b,*], Shuting Huang [c], Xiaoxue Wu [b], Ziyi Zhao [a], Xiaoting Liu [a], Chong Wu [a], Mengru Wang [a], Jialing Gao [b], Zunfu Ke [b], Xiaojing Ma [d], Weiling He [a,e,**]

[a] Department of Gastrointestinal Surgery, The First Affiliated Hospital, Sun Yat-Sen University, Guangzhou, Guangdong, 510275, China
[b] Institute of Precision Medicine, The First Affiliated Hospital, Sun Yat-Sen University, Guangzhou, Guangdong, 510275, China
[c] School of Public Health, Sun Yat-sen University, Guangzhou, Guangdong, 510275, China
[d] Department of Microbiology and Immunology, Weill Cornell Medicine, NY, 10065, USA
[e] School of Medicine, Xiang'an Hospital of Xiamen University, Xiamen University, Xiamen, Fujian, 361000, China

ARTICLE INFO

Keywords:
Chemoresistance
Ferroptosis
UBR5
Ubiquitination
SLC7A11

ABSTRACT

Chemoresistance remains a principal culprit for the treatment failure in colorectal cancer (CRC), especially for patients with recurrent or metastatic disease. Deciphering the molecular basis of chemoresistance may lead to novel therapeutic strategies for this fatal disease. Here, UBR5, an E3 ubiquitin ligase frequently overexpressed in human CRC, is demonstrated to mediate chemoresistance principally by inhibiting ferroptosis. Paradoxically, UBR5 shields oxaliplatin-activated Smad3 from proteasome-dependent degradation via Lys 11-linked poly-ubiquitination. This novel chemical modification of Smad3 facilitates the transcriptional repression of *ATF3*, induction of *SLC7A11* and inhibition of ferroptosis, contributing to chemoresistance. Consequently, targeting UBR5 in combination with a ferroptosis inducer synergistically sensitizes CRC to oxaliplatin-induced cell death and control of tumor growth. This study reveals, for the first time, a major clinically relevant chemoresistance mechanism in CRC mediated by UBR5 in sustaining TGFβ-Smad3 signaling and tuning ferroptosis, unveiling its potential as a viable therapeutic target for chemosensitization.

1. Introduction

Colorectal cancer (CRC) is the third most prevalent malignancy globally with high relapse and mortality rates [1]. Despite great progress in CRC therapeutics, chemotherapy remains the mainstay of treatment, particularly for patients with unresectable metastatic tumors or those who are unresponsive to immunotherapy. Oxaliplatin (Oxa) has been approved as a first- and second-line cornerstone chemotherapy for the treatment of resectable and advanced CRC, in combination with 5-fluorouracil (5-FU) and leucovorin (FOLFOX). Although FOLFOX and other Oxa-containing chemotherapeutic regimens have improved the response rates of patients with metastatic CRC [2], most patients eventually develop chemoresistance and recurrent disease, posing a tremendous obstacle in anticancer treatment. A recent meta-analysis of 25 studies reported that the 5-year disease-free survival (DFS) rate of patients with stage II CRC was 82.7 % without adjuvant chemotherapy and 79.3 % with adjuvant chemotherapy. For stage III disease, the percentages were even lower [3], indicating that only a small proportion of patients benefit from adjuvant chemotherapy, while 80 % of patients are exposed to unnecessary toxicity [4]. Hence, it is clinically important to elucidate the molecular mechanisms of chemoresistance and identify novel predictors of therapeutic outcomes to tailor anti-CRC treatment.

Multiple mechanisms, including drug efflux, enhanced DNA damage repairability, increased detoxifying enzyme levels, and reduced apoptosis, underlie the development of chemoresistance [5,6]. Recent studies have indicated that inducing ferroptosis, a type of regulated cell death characterized by lipid reactive oxygen species (ROS) accumulation and iron dependency, is a promising strategy to reverse resistance to cancer therapy, especially to overcome chemoresistance mediated by anti-apoptotic pathways [7–9]. Solute carrier family 7-member 11

* Corresponding author. Sun Yat-Sen University, Guangzhou, Guangdong 510275, China.
** Corresponding author. Sun Yat-Sen University, Guangzhou, Guangdong 510275, China.
E-mail addresses: songm7@mail.sysu.edu.cn (M. Song), hewling@mail.sysu.edu.cn (W. He).

https://doi.org/10.1016/j.redox.2024.103349
Received 7 July 2024; Received in revised form 24 August 2024; Accepted 8 September 2024
Available online 10 September 2024

(SLC7A11, xCT) is the catalytic subunit of the cystine/glutamate antiporter system that promotes cystine uptake and glutathione (GSH) biosynthesis, resulting in protection from oxidative stress and ferroptosis [10]. SLC7A11 is overexpressed in various human cancers, including CRC [11] and emerging evidence has revealed that suppressing SLC7A11 can inhibit tumorigenesis and sensitize CRC cells to chemotherapy by promoting ferroptosis [12–14].

Ubiquitin protein ligase E3 component n-recognin 5 (UBR5, also known as EDD) is a highly conserved HECT-domain E3 ubiquitin ligase essential for embryonic development in mammals [15,16]. It is frequently amplified and overexpressed in many cancer types [17–21], and is closely associated with advanced clinical stage, distant metastasis, and worse prognosis in patients. Our previous work demonstrated a pivotal role for UBR5 in promoting the aggressiveness of triple negative breast cancer (TNBC) and ovarian cancer [17–19,22]. In addition to its oncogenic properties in multiple cancers exemplified by their roles in the regulation of the DNA damage response [23], transcription [24], and apoptosis [25], UBR5 has been implicated in the resistance of breast and ovarian cancers to tamoxifen and cisplatin, respectively [26,27]. However, the mechanistic connections between UBR5 and drug resistance remain largely unexplored.

In the present study, we report for the first time that UBR5 mediates chemoresistance in CRC via SLC7A11-regulated ferroptosis. Targeting *UBR5* not only enhances ferroptosis susceptibility but also strongly potentiates the cytotoxic effects of Oxa. Mechanistically, abrogation of *UBR5* expedites the proteasome-dependent degradation of Oxa-activated Smad3 via impairment of Lys 11-linked polyubiquitination, thus repressing *SLC7A11* transcription and subsequently contributing to the chemosensitization of CRC. This study unveils a profound role of UBR5 in orchestrating chemoresistance through the TGFβ-Smad3 pathway and its novel downstream target SLC7A11. Targeting UBR5 emerges as a promising therapeutic strategy to ameliorate chemoresistance in CRC.

2. Results

2.1. High UBR5 expression correlates with chemoresistance in patients subjected to oxa-based therapy

To assess whether UBR5 is upregulated in CRC and has clinical relevance for chemoresistance, we analyzed *UBR5* mRNA/protein expression data from TCGA or cProSite databases and performed immunohistochemical (IHC) analysis of tissue microarrays (TMAs) containing 259 paired CRC and adjacent normal tissues from the First Affiliated Hospital at Sun Yat-Sen University (FAH-SYSU) (Supplementary Table 1). The results showed that UBR5 expression was significantly higher in TMA samples (Fig. 1A–C), which was further confirmed by the analysis of a collection of tumor samples of 29 CRC patients from FAH-SYSU (Fig. 1D). Increased UBR5 levels were significantly associated with more advanced stage and distant/lymph node metastasis (Fig. 1E and F), while low UBR5 expression was positively correlated with mismatch repair deficiency (dMMR)/microsatellite instability-high (MSI-H) status, a good prognostic factor in early-stage CRC and a novel predictor of sensitivity to immunotherapy-based treatments (Fig. 1G and H). These data suggest a potential prognostic value of UBR5 in patients with CRC.

Intriguingly, although no significant correlation between UBR5 expression and overall/recurrence-free survival (OS/PFS) was observed in the overall CRC patient population from TCGA and the public Gene Expression Omnibus database (Fig. 1I; Supplementary Figs. 1A and B), we found that high UBR5 expression was significantly associated with poor survival of patients receiving chemotherapy (Fig. 1J and K). To further investigate whether upregulated UBR5 confers CRC chemoresistance, we evaluated UBR5 status in 66 stage II/III CRC patients who received curative resection, followed by XELOX (capecitabine plus oxaliplatin) therapy (Supplementary Table 2). High UBR5 expression significantly correlated with short PFS in these patients (Fig. 1L and M). Furthermore, CRC patients receiving XELOX therapy with high UBR5 expression levels (H-score$\geq$ 70) displayed shorter OS than those with low UBR5 expression (H-score<70) (Fig. 1N). Collectively, these data demonstrate the clinical relevance of pretreatment UBR5 expression in predicting the response to subsequent Oxa-based therapy for CRC.

2.2. UBR5 deficiency enhances the sensitivity of CRC cells to oxa-induced cell death

To investigate the functional importance of UBR5 in CRC chemoresistance, we silenced *UBR5* in three CRC cell lines (SW1116, HCT116 and SW620) and assessed drug sensitivity. Knockdown of *UBR5* marginally affected cell propagation but notably reduced cell viability upon Oxa/5-Fu treatment (Fig. 2A–C; Supplementary Figs. 1C–G). While the co-administration of Oxa with 5-Fu or Capecitabine (Cape) demonstrated modest additive effects on cell death, the synergistic effects were greatly enhanced upon *UBR5* depletion (Supplementary Fig. 1E). Consistently, despite little difference in growth between SW1116-shNC and SW1116-sh*UBR5* xenograft tumors in nude mice, Oxa treatment markedly decreased the sh*UBR5*-tumor volume and weight *in vivo* (Fig. 2D and E). To better emulate the physiological tumor microenvironment, we established a patient-derived xenograft (PDX) model in which we observed that UBR5 deficiency enhanced the antitumor effect of Oxa (Fig. 2F–H; Supplementary Figs. 2A–C). Moreover, overexpression of UBR5 reduced sensitivity to Oxa (Supplementary Figs. 2D and E), suggesting that UBR5 aids in Oxa resistance in CRC. To further pinpoint the type(s) of cell death programs caused by UBR5 suppression during Oxa treatment, inhibitors of various cell death pathways, including apoptosis, ferroptosis, necroptosis, autophagy, and pyroptosis, were administered [28]. Notably, the ferroptosis inhibitor ferrostatin-1 (Fer) and the apoptosis inhibitor Z-VAD-FMK (VAD) largely reversed the decrease in cell viability, whereas the combination of Fer and VAD resulted in an almost complete recovery of cell viability both *in vitro* and *in vivo* (Fig. 2I–L; Supplementary Figs. 2F–H). Consistently, we observed elevated levels of apoptosis indicators in *UBR5*-knockdown cells treated with Oxa (Fig. 2M; Supplementary Figs. 2I and J). These data suggest that targeting UBR5 potentiates the cytotoxic effects of Oxa via both ferroptosis and apoptosis. Importantly, reintroduction of UBR5 into CRC-sh*UBR5* cells reduced their sensitivity to Oxa in terms of cell viability and ferroptosis susceptibility (Fig. 2N and O; Supplementary Fig. 3). Collectively, these data demonstrate that UBR5 depletion enhances the cytotoxic effects of Oxa in CRC cells.

2.3. UBR5 depletion promotes ferroptosis susceptibility in CRC cells

To elucidate the mechanisms underlying the *UBR5* deficiency-enhanced cytotoxic effects of Oxa, we performed transcriptome profiling using RNA-seq to explore the signaling pathways affected by UBR5 abrogation. Gene Ontology (GO) enrichment analysis revealed that genes involved in ion transport and regulation were significantly downregulated in Oxa-treated SW1116-sh*UBR5* cells. These genes play vital roles in maintaining intracellular iron homeostasis and are closely associated with ferroptosis (Fig.

3A). Additionally, we found significant enrichment of oxidoreductase activity in the Oxa-sh*UBR5* group (Fig. 3B). Thus, we assessed lipid oxygen species (ROS) production using C11-BODIPY and evaluated mitochondrial damage through transmission electron microscopy (TEM) in CRC cells following exposure to Oxa or RSL3.Oxa treatment resulted in markedly increased levels of lipid peroxidation, a hallmark of ferroptosis, in *UBR5* deficient cells, but not in the control group marked increase in lipid ROS formation. Furthermore, UBR5 suppression dramatically augmented RSL3-induced lipid peroxidation, indicating that UBR5 inhibition promotes ferroptosis (Fig. 3C and D). TEM revealed that *UBR5* deficient CRC cells displayed more pronounced mitochondrial morphological alterations compared to shNC cells when treated

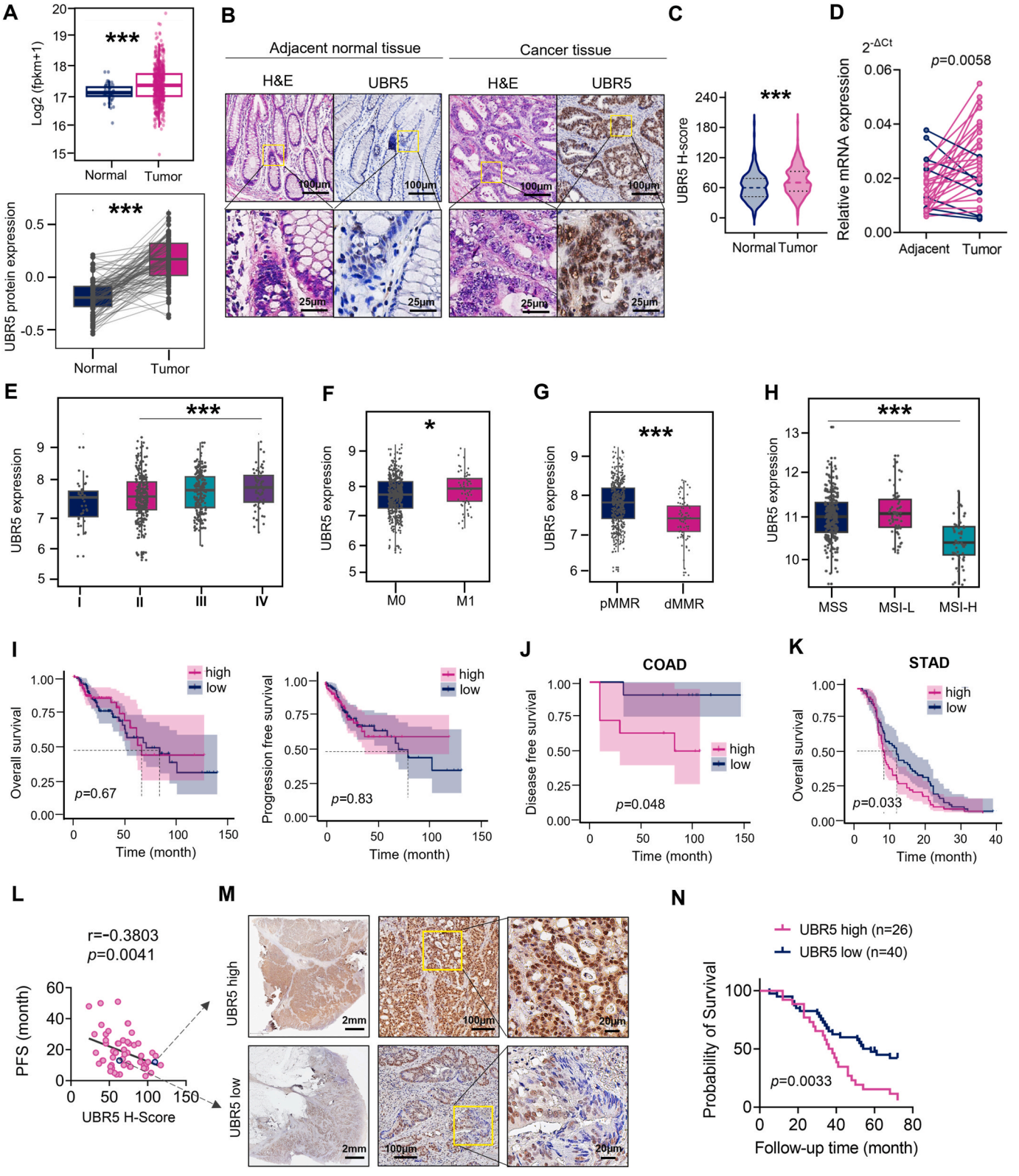

(caption on next page)

Fig. 1. UBR5 is upregulated in human CRC and positively correlates with chemoresistance.
A.*UBR5* mRNA levels in CRC specimens (n = 603) compared to normal colon tissues (n = 48) based on the TCGA database (upper) and paired protein expression based on cProSite database (lower). The *p* value was determined by Wilcoxon signed ranks test.
B.Representative H&E and UBR5 IHC staining in CRC and corresponding adjacent normal tissues. Scale bars:100 μm. Lower panels are × 5 magnification of the square areas on the upper panels.
C.Quantification of UBR5 IHC staining with human colorectal tumor microarrays (TMAs) from 259 patients.
D.mRNA expression of *UBR5* in paired CRC tissues was assessed by qPCR (n = 29).
E-G.*UBR5* mRNA expression in different TNM classification(**E**), distant metastasis (**F**), and mismatch repair status (**G**) of CRC based on the data from GSE39582 (n = 585)."
H.*UBR5* mRNA expression in CRC with different microsatellite stability status from TCGA colon and rectal cancer database (n = 434).
I.Kaplan–Meier plot showing the correlations between UBR5 expression and overall survival (OS) (left) and progression free survival (PFS) (right) in CRC patients from the TCGA database (n = 434).
J-K. Correlations of *UBR5* mRNA expression with disease free survival of CRC patients subjected to chemotherapy (GSE143985, n = 22) (**J**) and OS of stomach cancer patients received cisplatin/fluorouracil combination chemotherapy (GSE14210, n = 118) (**K**) were analyzed by Kaplan–Meier plotter
L, **M.**UBR5 IHC staining (**M**) and Pearson correlation analysis between UBR5 expression and PFS (**L**) in CRC patients subjected to XELOX.
N. Kaplan-Meier plot of the correlation between UBR5 expression and overall survival of patients subjected to XELOX.
The *p* values of C, D, E, F, G, and H were determined with unpaired two-side Student's *t*-test. The *p* values of I, J, K and N were determined by log-rank test. $*p < 0.05$, $***p < 0.001$.

with Oxa, characterized by shrunken mitochondria with ruptured cristae and increased membrane density (Fig. 3E). Moreover, GO analysis identified significant enrichment in pathways related to metabolic processes. Further KEGG pathway analysis revealed that UBR5 was highly correlated with lipid metabolism, especially fatty acid and cysteine/methionine metabolism, both of which are closely related to ferroptosis (Fig. 3F). Cysteine is the rate-limiting metabolite for glutathione (GSH) biosynthesis, which scavenges ROS and inhibits ferroptosis [29]. As expected, UBR5 depletion reduced GSH/GSSG ratio while promoted lipid ROS production, as evidenced by elevated levels of malondialdehyde (MDA), the aldehyde secondary products of lipid peroxidation (Fig. 3G and H; Supplementary Fig. 4A). In line with the above observations, a few ferroptosis-executing genes were upregulated (including *ATF3, MAP1LC3B, VDAC2, SAT1*), while a set of ferroptosis negative regulation (FNR) genes were downregulated in Oxa-treated SW1116-sh*UBR5* cells, including *SLC7A11*, *NFE2L2*, *FTH1*, *GCLC*, *HELLS* and its downstream targets *SCD1/FADS2* (Fig. 3I). Together, these data suggest that loss of UBR5 promotes Oxa-triggered ferroptosis by perturbing redox and GSH homeostasis.

2.4. Targeting UBR5 augments the benefit of chemotherapy synergistically with RSL3

Augmentation of ferroptosis has been shown to reverse chemoresistance in cancer [9]. Given that targeting *UBR5* sensitizes CRC cells to the ferroptosis inducer RSL3 (Fig. 3C and D), we reasoned that RSL3 administration together with UBR5 inhibition may synergistically augment the cytotoxicity of Oxa. *In vitro* cell death was significantly increased in CRC-sh*UBR5* cells upon RSL3 treatment, as manifested by the increase in lipid ROS levels (Fig. 4A; Supplementary Fig. 4B). Moreover, RSL3 strongly intensified the cytotoxic effects of Oxa, exacerbating the ferroptotic mitochondrial alterations in CRC-sh*UBR5* cells (Fig. 4B and C; Supplementary Figs. 4C and D). Administration of Oxa or RSL3 alone moderately inhibited SW1116-shNC tumor growth *in vivo*, and there was a slight added benefit of RSL3 to Oxa treatment. In sharp contrast, the administration of Oxa or RSL3 dramatically suppressed the growth of SW1116-sh*UBR5*. Strikingly, the greatest tumor inhibition was observed when Oxa was combined with *UBR5* depletion and RSL3, highlighting the synergy between UBR5 inhibition and RSL3 in chemosensitization (Fig. 4D–F; Supplementary Fig. 4E). Analysis of the intratumoral concentration of MDA confirmed that both Oxa and RSL3 treatment resulted in more lipid ROS accumulation in SW1116-sh*UBR5* tumors, with the highest level in combinatory treatment (Fig. 4G). It is worth noting that body weight did not differ significantly between the control and treatment groups, supporting the general tolerability of the combination in mice (Supplementary Fig. 4F). In addition, pathological analysis revealed increased necrosis and fibrosis in UBR5-depleted tumors, as well as reduced cell proliferation (Ki67), increased lipid ROS levels (4-HNE staining), and enhanced cell death (TUNEL staining) in response to antitumor therapies. Similarly, the combination of Oxa and RSL3 achieved the best suppressive effects against *UBR5*-deficient tumors (Fig. 4H and I). Of note, *UBR5*-deficient tumors exhibit higher apoptotic indexes (with elevated Bax staining but reduced Bcl-2 signal) than control tumors after Oxa treatment, indicating that apoptosis also contributes to UBR5 suppression-mediated chemosensitivity. These data together demonstrate that targeting UBR5 in combination with a ferroptosis inducer can synergistically enhance chemosensitivity, leading to potent tumor suppression.

2.5. UBR5 silencing potentiates the cytocidal effect of oxa via SLC7A11 repression

To identify the important ferroptosis regulators linked to UBR5-mediated chemoresistance, we examined the transcription of several ferroptosis-related genes based on RNA-seq data (Fig. 3I). UBR5 deficiency led to downregulation of *SLC7A11* in CRC cells, which was exacerbated by Oxa treatment. Nevertheless, only slight alterations were observed in the mRNA and protein expression levels of other ferroptosis regulators, including SCD1, FTH1, GPX4 and HELLS between the shNC and sh*UBR5* groups (Fig. 5A and B; Supplementary Figs. 5A and B), highlighting the prominence of SLC7A11 in UBR5-regulated ferroptosis. As a key importer of cystine that facilitates GSH biosynthesis, SLC7A11 enables cancer cells to bolster their antioxidant defenses and evade ferroptosis. Its transcription is tightly controlled under basal and stress conditions by multiple factors, such as NRF2, P53, ATF3, and BAP1 [30]. However, only marginal difference in the NRF2, BAP1 and P53 levels was found between control and sh*UBR5* groups upon Oxa treatment. Notably, consistent with RNA-seq findings (Fig. 3I), UBR5 deficiency consistently upregulated ATF3 expression at both mRNA and protein levels, which became more pronounced following Oxa treatment (Fig. 5A and B). ATF3 was reported to promote ferroptosis through suppression of *SLC7A11* transcription [31]. We observed elevated SLC7A11 expression in *UBR5*-deficient CRC cells after ATF3 knockdown (Supplementary Fig. 5C). IHC analysis of human CRC TMAs also validated the strong positive correlation between UBR5 and SLC7A11 expression ($r = 0.493$, $p < 0.0001$), and a negative correlation between UBR5 and ATF3 expression ($r = -0.111$, $p = 0.043$) (Fig. 5C and D), establishing an important clinical connection between UBR5 and well-defined ferroptosis regulators. We then sought to functionally link SLC7A11 to UBR5-mediated chemoresistance by reintroducing SLC7A11 into sh*UBR5* CRC cells (Fig. 5E). *In vitro*, overexpression of SLC7A11 in *UBR5*-deficient CRC cells largely restored cell viability and mitigated Oxa-induced lipid peroxidation to control levels (Fig. 5F–I; Supplementary Figs. 5D–F). Additionally, the attenuated tumor growth

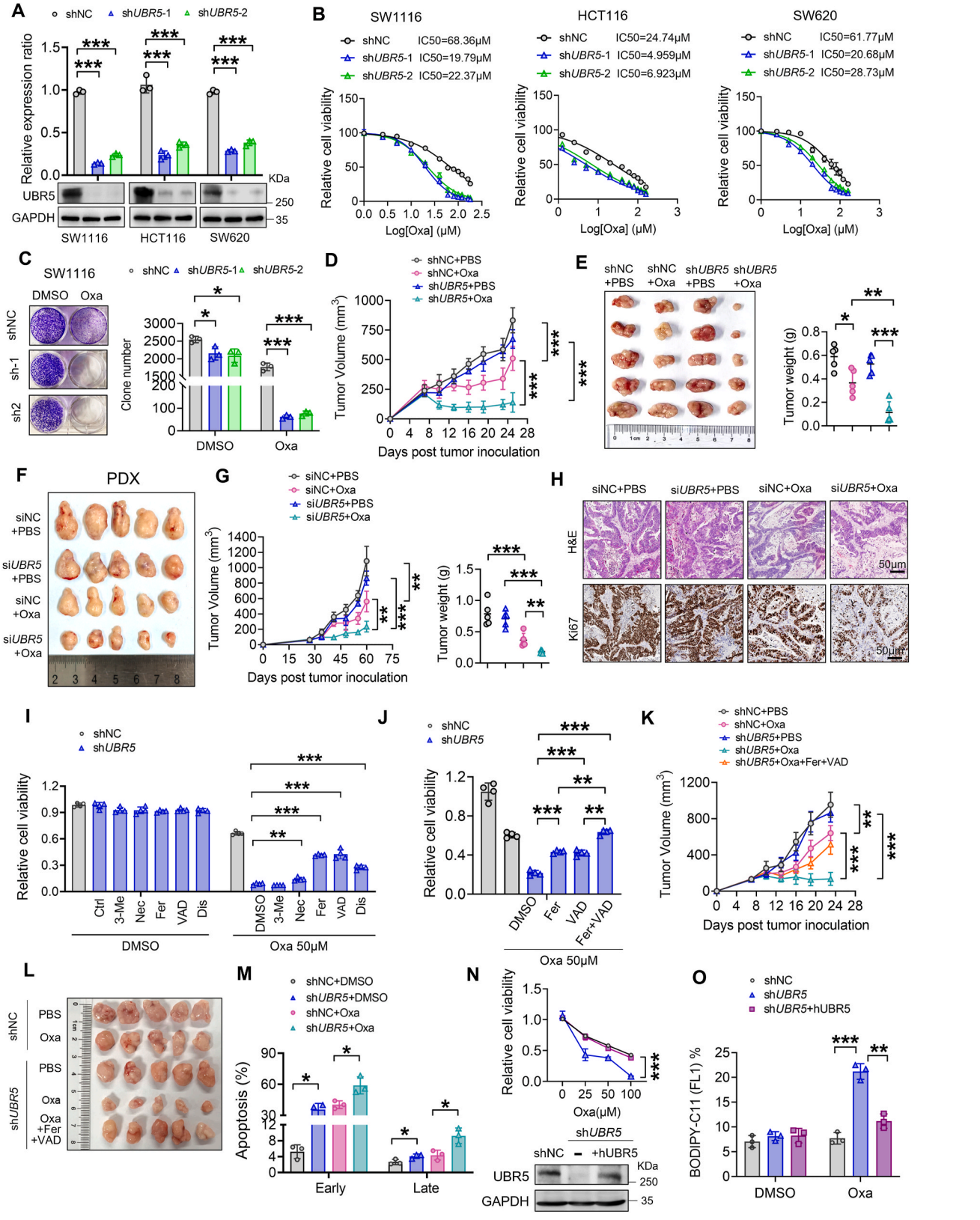

(caption on next page)

Fig. 2. UBR5 contributes to Oxa-based chemoresistance in CRC.
A.qPCR analysis of the relative *UBR5* mRNA levels and western blot analysis of UBR5 protein expression in shNC and CRC-sh*UBR5* cells.
B.Cell viability of shNC and CRC-sh*UBR5* cells treated with Oxa at indicated concentrations for 48h.
C.Representative images (left) and quantification (right) of clonogenic assay with 2500 SW1116 cells/well.
D, E. Representative images (**E**, left) and statistical analysis of xenograft tumor volumes (**D**) and weights (**E,** right) in nude mice after implantation of SW1116 (shNC&sh*UBR5*) cells, followed by i.p injection of Oxa (7.5 mg/kg) or PBS (n = 5 mice per group).
F-G. Representative images (**F**) and statistical analysis of tumor volumes (**G**, left) and weights (**G,** right) in CRC PDX models, after intratumoral injection of siRNAs (siNC or si*UBR5*) and i.p injection of Oxa (7.5 mg/kg) or PBS (n = 5 mice per group).
H.Representative H&E and IHC staining images of Ki67 in tumor sections from CRC PDX model.
I.Cell viability of shNC and shUBR5 SW1116 cells with or without Oxa (50 μM) for 48h in combination with the 3-methyladenine (3-Me, 1 μM), Necrostatin (Nec, 20 μM), Ferrostatin-1(Fer, 10 μM), Z-VAD-FMK (VAD, 25 μM) and Disulfiram (Dis, 1 μM).
J.Cell viability of shNC and shUBR5 SW1116 cells with or without Oxa (50 μM) for 48h in combination with Fer, VAD, and Fer + VAD.
K, L. Representative images (**L**) and statistical analysis of xenograft tumor volumes (**K**) in nude mice after implantation of SW1116 (shNC&sh*UBR5*) cells, followed by i.p injection of Oxa (7.5 mg/kg), Fer (5 mg/kg), and VAD(5 mg/kg) (n = 5 mice per group).
M.SW1116 (shNC&shUBR5) cells were treated with Oxa (25 μM) for 24h, the percentage of apoptotic cells were assessed.
N.Cell viability of UBR5 reconstituted SW1116-shUBR5 cells treated with Oxa at indicated concentrations for 48h (upper). UBR5 protein expression was detected by western blot (lower).
O.The percentage of BODIPY™ 581/591C11^{+} SW1116 cells treated with Oxa (25 μM) for 24h.
Data are presented as mean ± SD. The *p* values of D, G, K, and N were determined by two-way ANOVA test. The *p* values of A, C, E, I, J, M, and O were determined with unpaired two-side Student's *t*-test. $*p < 0.05$, $**p < 0.01$, $***p < 0.001$

of SW1116-sh*UBR5* cells after Oxa administration was rescued *in vivo* by SLC7A11 restoration, suggesting that UBR5-regulated chemoresistance is dependent on SLC7A11 (Fig. 5J and K; Supplementary Figs. 5G and H). Furthermore, treatment with the antioxidant N-acetyl-$_{L}$-cysteine (NAC) reduced lipid peroxidation and recovered the viability of Oxa--sh*UBR5* CRC cells (Fig. 5L and M; Supplementary Figs. 5I–L). Altogether, these data demonstrate that UBR5 dictates ferroptosis sensitivity by controlling the ATF3-SLC7A11 transcriptional axis, thereby sustaining chemoresistance in CRC.

2.6. UBR5 transcriptionally regulates ATF3/SLC7A11 principally via Smad3

UBR5 regulates gene transcription by targeting nuclear receptors or transcriptional complexes via its E3 ubiquitin ligase [32]. We then analyzed the potential UBR5 substrates predicted using the Ubibrowser website (Supplementary Fig. 6A) and found that several proteins relevant to the TGF-β signaling pathway were among the top 20 predicted substrates, including TGFBR2, Smad4, Smad5, and Smurf1. Smad proteins are a family of structurally similar molecules that play pivotal roles in the TGF-β superfamily intracellular cascade. Interestingly, we observed that UBR5 depletion in CRC cells moderately decreased the protein levels of Smad2/3/4, which were further reduced in response to Oxa or TGF-β (Fig. 6A–C; Supplementary Figs. 6B–D), suggesting that targeting *UBR5* synergizes with chemotherapy to impair TGF-β-Smad signaling. However, the expression of other effectors in the TGF-β signaling pathway, such as TGFBR2, Smad5, Smurf1 and Smurf2, were not affected by UBR5 depletion (Supplementary Fig. 6E). We then sought to determine the role of Smads in UBR5-regulated *ATF3/SLC7A11* transcription. Knockdown of Smad2/3/4 induced *ATF3* transcription but suppressed *SLC7A11* mRNA expression to varying degrees. Among them, Smad3 appeared to be the most important modulator of *ATF3/SLC7A11* transcription (Fig. 6D and E; Supplementary Figs. 6F and G). Highly positive correlations between Smad3 and SLC7A11 were also ascertained by TMA-based analyses of human CRC samples (Fig. 6F). Luciferase reporter assays were performed to assess the transcriptional effects of UBR5 on *SLC7A11* and *ATF3* in CRC cells. The loss of *UBR5* resulted in decreased *SLC7A11* promoter activity, whereas it enhanced the transcriptional activity of the *ATF3* promoter, both of which were reversed upon Smad3 reintroduction into CRC-sh*UBR5* cells (Fig. 6G). Moreover, chromatin immunoprecipitation (ChIP)-qPCR analyses revealed enhanced recruitment of Smad3 binding to both *SLC7A11*(-1to-179) and *ATF3* promoters (−691to-812) (Fig. 6H–K). Consistently, re-expression of Smad3 in the sh*UBR5* group rescued SLC7A11 expression and reversed the increase in ATF3 expression (Fig. 6L). Accordingly, the viability of SW1116-sh*UBR5* cells in the presence of Oxa was partially restored, and the cells exhibited enhanced clonogenic capacity and reduced lipid ROS accumulation (Fig. 6M–O; Supplementary Figs. 6H and I). Taken together, these results indicate that UBR5 regulates chemoresistance partially through the Smad3/SLC7A11 axis by promoting *SLC7A11* transcription while suppressing *ATF3* transcription.

2.7. UBR5 enhances the protein stability of nuclear smads

To determine how Smad proteins are regulated by UBR5, we conducted coimmunoprecipitation (Co-IP) and found physical interactions between endogenous Smad2/3 and UBR5 in CRC cells (Fig. 7A), and between exogenously introduced, Strep-tagged UBR5 and Flag-tagged Smad3 in HEK293T cells (Fig. 7B). Moreover, the interaction between UBR5 and Smad3 was augmented by TGF-β treatment (Fig. 7C). In control CRC cells, cytosolic Smad2/3 was phosphorylated and translocated to the nucleus in response to Oxa (Fig. 7D and E; Supplementary Fig. 6J). Endogenous UBR5 showed nuclear staining and colocalization with Smad2/3. A similar subcellular distribution of Smad2/3 was observed in CRC-sh*UBR5* cells upon Oxa treatment, but the loss of UBR5 dramatically reduced the total protein levels of Smad2/3. Moreover, the half-life of Smad2/3 was markedly reduced in the absence of UBR5 in CRC cells treated with the protein synthesis inhibitor cycloheximide (CHX) (Fig. 7F and G), suggesting that UBR5 maintained Smad2/3 protein stability. Furthermore, elevated accumulation of Smad2/3, as well as Smad4 (while not TGFBR2, Smad5, and Smurf1/2) was observed in MG132-treated but not BafA1(an autophagy inhibitor)-treated CRC-sh*UBR5* cells, indicating that UBR5 regulates Smad2/3/4 stability via the ubiquitin-proteasome system (Fig. 7H; Supplementary Fig. 6K). Additionally, treatment with ITD-1, a specific blocker of Smad2/3 phosphorylation, strongly increased their protein levels in Oxa-treated CRC-sh*UBR5* cells, as did the selective Smad3 phosphorylation inhibitor SIS3–HCl (Fig. 7I–K; Supplementary Fig. 6L). These results indicate that UBR5 protects Oxa-induced Smad2/3 from destruction via the 26S proteasome pathway in a phosphorylation-dependent manner.

2.8. UBR5 stabilizes Smad3-SLC7A11 axis via Lys 11-dependent ubiquitination

Timely turnover of activated Smad2/3 is mediated mainly by SMAD ubiquitination regulatory factor 1/2(Smurf1/2)-dependent degradative polyubiquitylation [33]. However, *UBR5* depletion did not significantly alter Smurf1 or Smurf2 expression in CRC cells (Supplementary Fig. 6E), suggesting that UBR5 may enhance the protein stability of Smad3 via Smurf1/2-independent ubiquitination. In a cell-based assay, polyubiquitin levels of Flag-tagged Smad3 were enhanced by Strep-UBR5

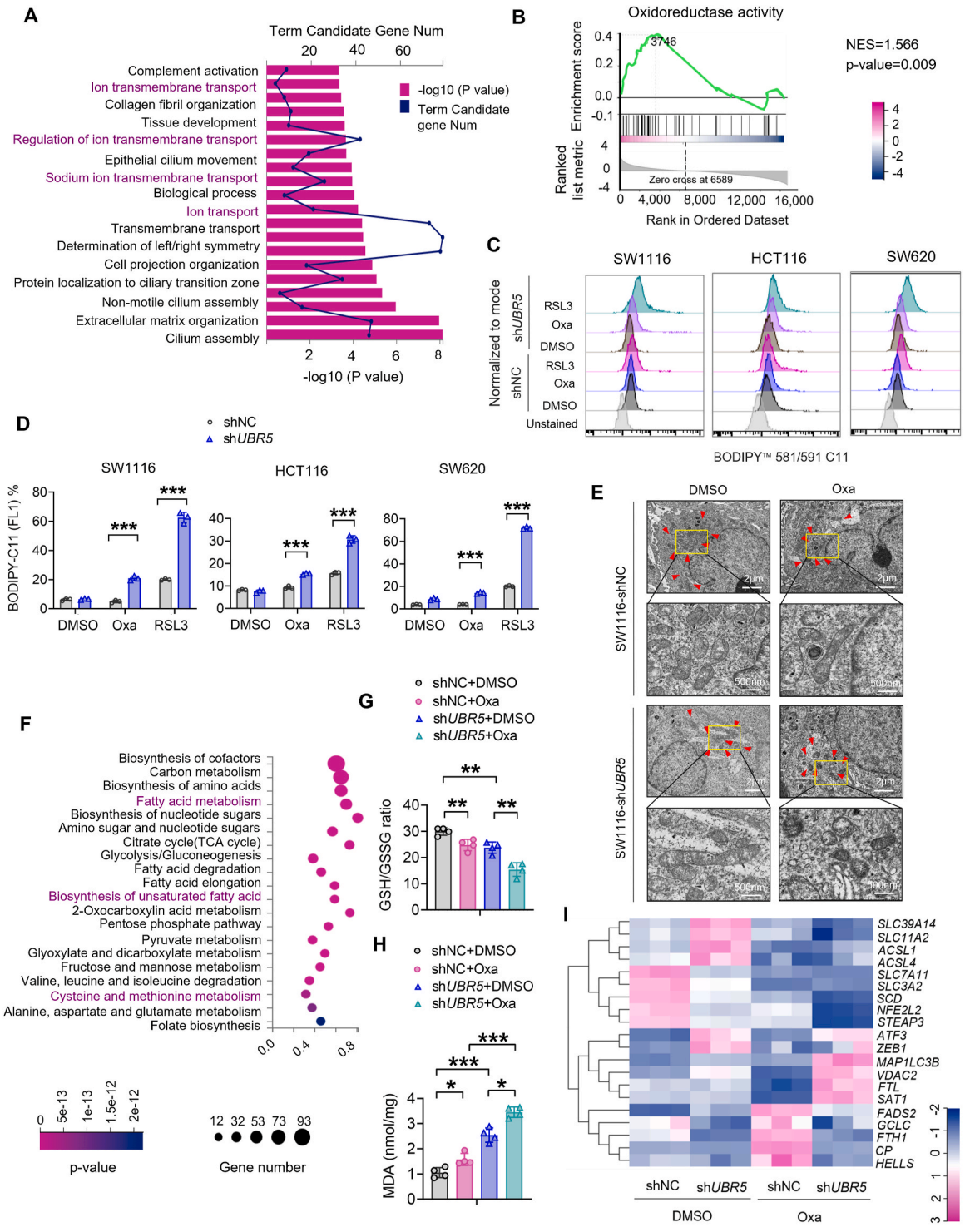

Fig. 3. Targeting UBR5 promotes ferroptosis susceptibility in CRC cells

A.Gene ontology (GO) enrichment analysis of down-regulated genes under Oxa treatment (25 μM, 48h) in sh*UBR5* group compared with shNC group.

B.Gene set enrichment pathway analysis (GSEA) showing the significant enrichment of the GO gene sets in Oxa-treated SW1116-sh*UBR5* cells.

C, D Representative FACS images (**C**) and quantified values (**D**) of the lipid ROS levels in HCT116/SW620 (shNC&sh*UBR5*) cells treated with Oxa (25 μM) or RSL3 (5 μM) for 24h.

E.Representative TEM images of SW1116 (shNC&shUBR5) cells after the indicated treatment with Oxa (25 μM) for 24h.

F.KEGG pathway analysis of differentially expressed genes (DEGs) in metabolic process between shNC and shUBR5 SW1116 cells upon Oxa treatment.

G, H.Intracellular GSH/GSSG ratios (G) and cellular concentrations of MDA (H) were evaluated in SW1116 cells (shNC&shUBR5) with or without Oxa (25 μM, 48h) treatment.

I.Heat map representation of differentially expressed ferroptosis-related genes between shNC and shUBR5 SW1116 cells with or without treatment.

Data of D, G, and H are representative of three independent experiments. Data are presented as mean ± SD, unpaired two-side Student's *t*-test. $^{*}p < 0.05$, $^{**}p < 0.01$, $^{***}p < 0.001$

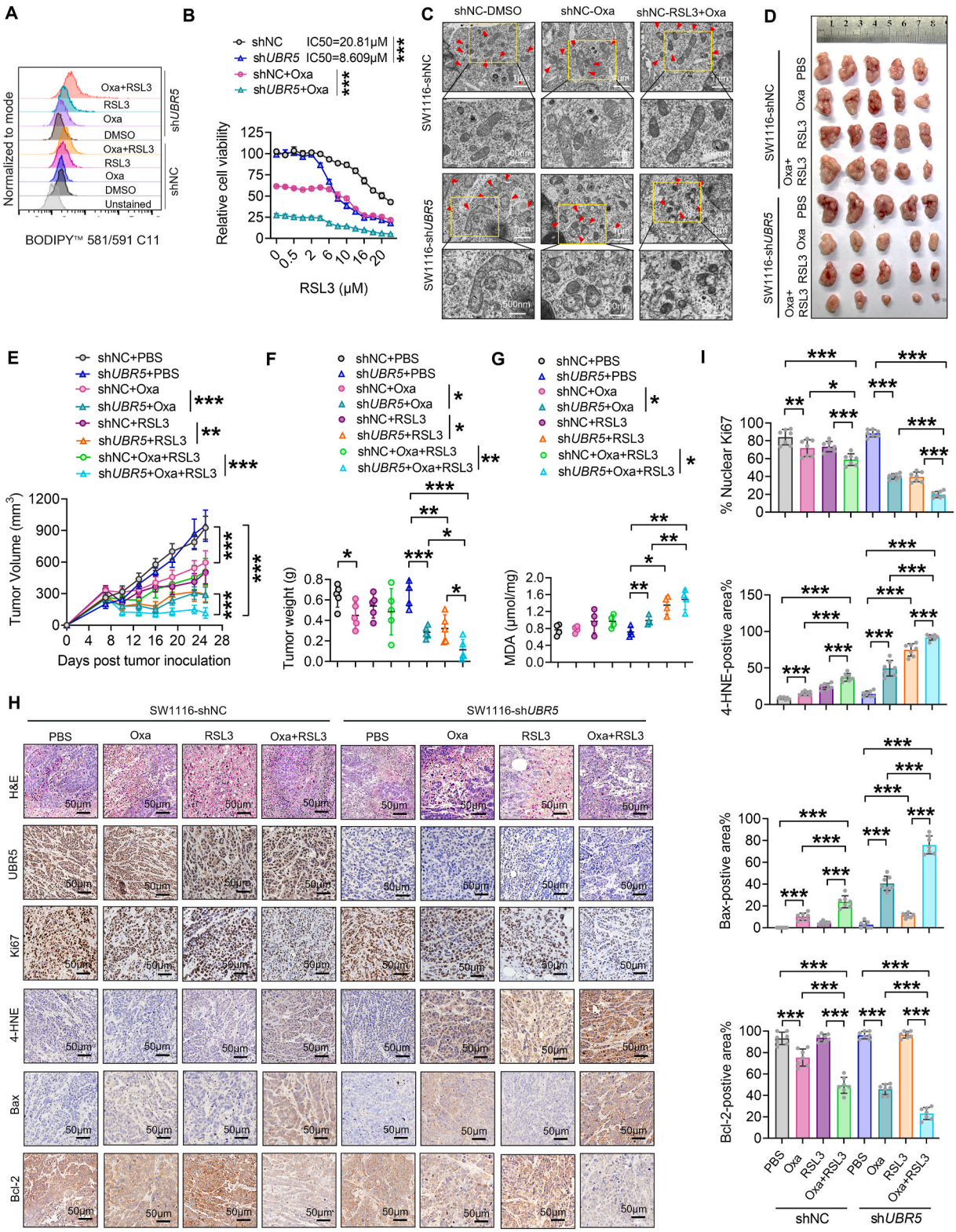

Fig. 4. Targeting UBR5 in combination with RSL3 synergistically enhances chemosensitivity in CRC.
A.Representative FACS images of the lipid ROS levels in SW1116 (shNC&sh*UBR5*) cells treated with Oxa (25 μM) and/or RSL3 (5 μM) for 24h.
B.Dose-response curves of SW1116 cells (shNC and sh*UBR5*) treated with RSL3 at the indicated concentrations with or without Oxa (25 μM) for 48h.
C.Representative TEM images of SW1116 (shNC&sh*UBR5*) cells after the indicated treatment with Oxa (25 μM) and RSL3 (5 μM) for 24h.
D-G. Tumors from the xenograft mouse model were resected (**D**) and tumor weights (**F**), intratumor MDA levels (**G**) were measured on day 25 post tumor inoculation.
E, Statistical analysis of tumor volume in nude mice.
H, I. Representative H&E and IHC staining images (**H**) and quantification (**I**) of UBR5, Ki67,4-HNE, Bax, and Bcl-2 staining in xenograft tumor sections.
Data are presented as the mean ± SD. The *p* values of B, E were determined by two-way ANOVA test. The *p* values of F, G, I were determined with unpaired two-side Student's *t*-test. $*p < 0.05$, $**p < 0.01$, $***p < 0.001$

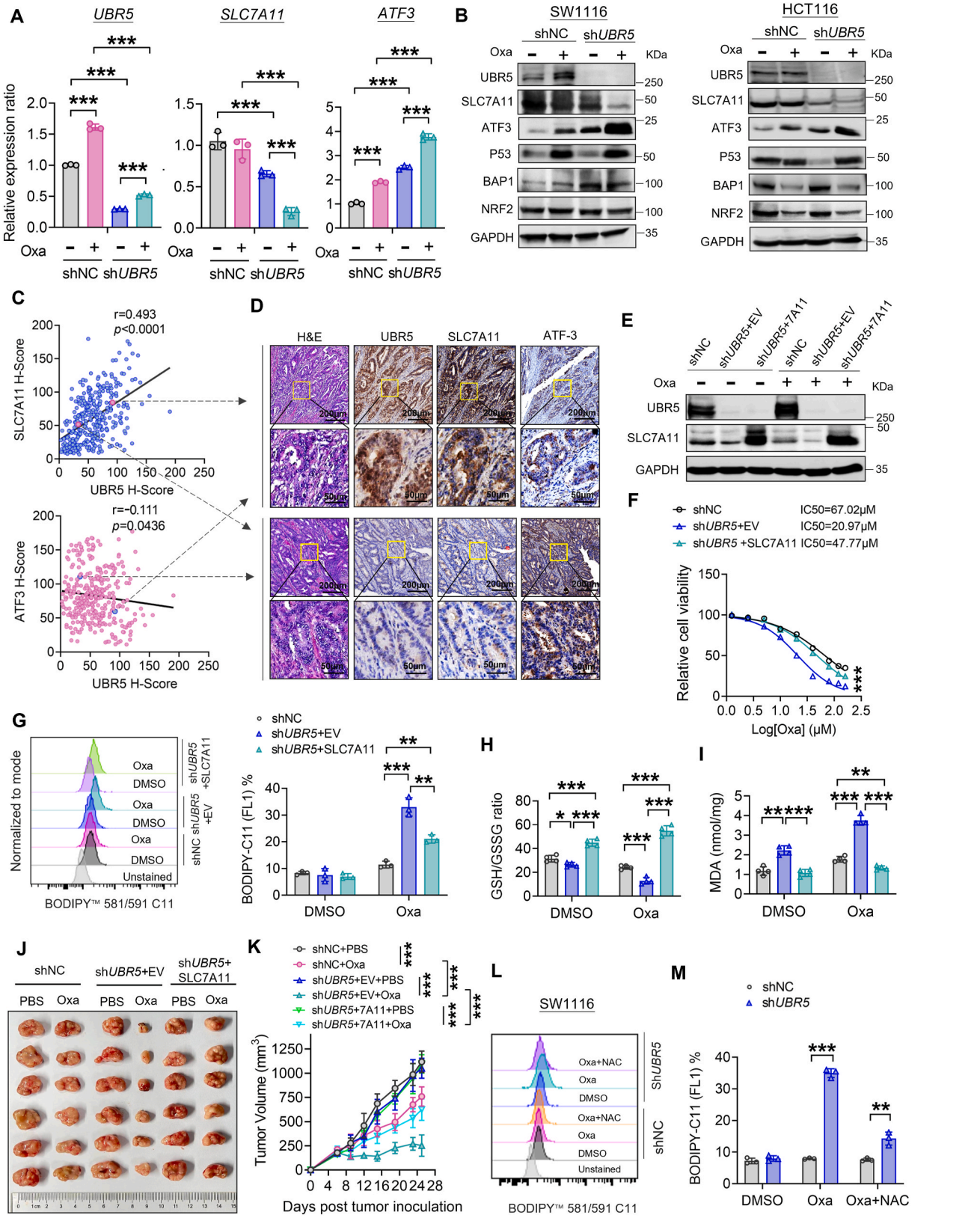

(caption on next page)

Fig 5. UBR5 regulates chemoresistance of CRC in a SLC7A11-depdendent manner.
A, B.q-PCR analysis of the relative *UBR5*, *SLC7A11*, *ATF3* mRNA levels (**A**) and western blot detection of the UBR5, SLC7A11, ATF3, P53, BAP1, NRF2 and GAPDH protein levels
(**B**) in CRC (shNC&sh*UBR5*) cells with or without Oxa treatment (25 μM, 48h).
C.Correlation assessed by Pearson correlation analysis and linear regression analysis between UBR5 and SLC7A11expression, C. Correlation assessed by Pearson correlation analysis and linear regression analysis between UBR5 and SLC7A11expression (upper), UBR5 and ATF3 expression in the human CRC TMAs (n = 329)
D.Representative H&E and IHC staining of UBR5, SLC7A11, and ATF3 in human CRC TMAs.
E.Overexpression of SLC7A11 in SW1116-shUBR5 cells was verified by western blot.
F.Cell viability of shNC, shUBR5, and shUBR5+SLC7A11 SW1116 cells treated with Oxa at indicated concentrations for 48h.
G.Representative FACS images and lipid ROS levels in indicated SW1116 cells with or without Oxa treatment.
H, I. Intracellular GSH/GSSG ratios (H) and cellular concentrations of MDA (I) were evaluated in SW1116 cells (shNC&shUBR5&shUBR5+SLC7A11) with or without Oxa (25 μM, 48h) treatment.
J, K.Representative images (J) and statistical analysis of xenograft tumor volumes (K) in nude mice after implantation of SW1116 (shNC&sh*UBR5*&-sh*UBR5*+SLC7A11) cells, followed by i.p injection of Oxa (7.5 mg/kg) or PBS (n = 6 mice per group).
L, M. Lipid ROS levels in SW1116 (shNC&sh*UBR5*) cells treated with 25 μM Oxa combined with 2.5 mM NAC for 24h.
Data are presented as mean ± SD. The *p* values of F and K were determined by two-way ANOVA test. The *p* values of A, G, H, I, M were determined with unpaired two-side Student's *t*-test. $^{**}p < 0.01$, $^{***}p < 0.001$

overexpression in the absence (lane 3 vs. lane 5) and presence (lane 4 vs. lane 6) of MG132, indicating that UBR5-mediated ubiquitination does not render Smad3 unstable. In contrast, it protected Smad3 from proteasome-mediated degradation (Fig. 8A). To classify the UBR5-mediated Smad3 polyubiquitin chain linkage, a series of ubiquitin mutant isoforms were used to reveal that UBR5's ability to ubiquitinate Smad3 was impaired by the K11R mutation (Fig. 8B). UBR5 specifically enhanced the K11-linked polyubiquitination of Smad3 but had no impact on K29-linked polyubiquitination (Fig. 8C). Moreover, the K11R mutant led to decreased Flag-Smad3 levels, as well as downstream SLC7A11 and Snail expression, compared to wild-type ubiquitin or other mutants in HEK293T cells (Fig. 8D), suggesting that UBR5 enhances Smad3 protein stability via K11-linked polyubiquitination. In contrast, overexpression of UBR5's E3 ligase catalytic mutant (UBR5-C2768A) did not increase the ubiquitination level of Smad3 or the protein levels of Smad3, SLC7A11, and Snail, supporting that UBR5 stabilizes Smad3 via its E3 ligase activity (Fig. 8E and F).

To identify ubiquitinated lysine(K) residues in Smad3, we constructed six Lys to Arg mutants (K53R, K81R, K333R, K341R, K378R, and K409R) according to prediction by the GPS-Uber database (Supplementary Fig. 6M). Co-IP results revealed that K333R and K378R mutations largely disrupted UBR5-mediated ubiquitination (Fig. 8G). We then generated a K333R/K378R double mutant Smad3 construct and observed a complete loss of UBR5-mediated ubiquitination and stabilization. Relative to wild-type Smad3, the K333R/K378R mutant significantly suppressed SLC7A11 and Snail expression (Fig. 8H and I). $Smad3^{K333R/K378R}$ was degraded through the proteasomal pathway, mainly via K48-linked ubiquitination (Fig. 8J). Altogether, these results demonstrate that Lys^{333} and Lys^{378} are pivotal target residues in Smad3 for UBR5-mediated K11 ubiquitination and protein stabilization.

3. Discussion

Our study was inspired by the clinically observed correlation between high UBR5 expression and chemoresistance in CRC patients validated by clinical meta-databases and our internal patient sample collection. We then delved into the mechanistic insights of UBR5's pivotal role in mediating chemoresistance as a ferroptosis suppressor. Diverging from the classical function of E3 ligases in target protein degradation, UBR5 intriguingly acts as a stabilizer of the Smad3-SLC7A11 axis by facilitating K11-linked polyubiquitination of Oxa-activated Smad3. This novel post-translational modification promotes the transcriptional repression of ATF3, induces SLC7A11 expression, and inhibits ferroptosis, thereby contributing to chemoresistance. We further demonstrated the translational value of our findings by analyzing human CRC samples, which confirmed strong positive correlations between UBR5, Smad3 and SLC7A11 expression. Consistently, targeting UBR5 with a ferroptosis inducer synergistically sensitizes CRC cells to Oxa-induced cell death and enhances tumor growth control. This study not only reveals UBR5 as a crucial bridging molecule connecting chemoresistance and ferroptosis, shedding light on new chemosensitization strategies, but also advances our understanding of ubiquitination-evoked intracellular signaling networks in fine-tuning ferroptosis.

UBR5 amplification and overexpression are frequently observed in many cancer types. Unlike breast and ovarian cancer, where high UBR5 expression is linked to poor patient prognosis [17–19], no correlation was observed between its expression and overall CRC patient survival based on publicly available databases (Fig. 1I). Strikingly, analyses of the clinical meta-database and our internal patient sample collection (n = 66) from FAH-SYSU unanimously revealed that high UBR5 expression was significantly correlated with chemoresistance (Fig. 1L–N). Moreover, our study demonstrated, for the first time, that UBR5 deficiency sensitizes CRC to chemotherapy primarily by inducing ferroptosis in a SLC7A11-dependent manner, highlighting the clinical significance of UBR5 in mediating CRC chemoresistance. This conclusion is further reinforced by the observation of a strong positive correlation between UBR5 and SLC7A11 expression in human TMA prepared from CRC patients in FAH-SYSU (n = 259). Mechanistically, UBR5-dependent stabilization of Smad3 not only directly promotes SLC7A11 transcription, but also suppresses the mRNA expression of ATF3, a negative regulator of SLC7A11 [31]. In hepatocellular carcinoma cell lines, Smad3 participates in TGF-β1-mediated repression of SLC7A11 [34]. Therefore, Smad3 may exert divergent effects on SLC7A11 transcription depending on the tumor type, consistent with its widely reported context-specific regulation of gene expression [35–37] (Supplementary Fig. 6B). Notably, our study identified the direct genomic binding regions of Smad3 on the SLC7A11 and ATF3 gene promoters by ChIP assay. Apart from transcriptional regulation, the expression of SLC7A11 is also regulated post-translationally, particularly through ubiquitin-proteasome-dependent mechanisms in human cancers. Several ubiquitin ligases and deubuquitinases, such as OTUB1, HECTD3, and β-TrCP1/2, have been identified as regulators of SLC7A11 ubiquitination and stability in CRC [38–40]. Whether UBR5 directly modulates SLC7A11 protein expression via its E3 ligase activity remains an open question that warrants further exploration.

UBR5 has emerged as a critical regulator in suppressing apoptotic signaling within tumor cells. Depletion of UBR5 was identified to enhance the susceptibility of breast cancer cells to Fas-ligand mediated apoptosis [38]. Moreover, in MYC-amplified, p53-mutant breast cancer cells, UBR5 was reported to suppress Myc-mediated apoptosis priming and protect these tumor cells from drug-induced apoptosis [25]. It has also been shown to confer cisplatin resistance in OC cells by down-regulating proapoptotic MOAP-1 protein [39]. *In vivo*, the loss of UBR5 has been observed to inhibit tumor metastasis by inducing p53-mediated apoptosis in mouse models of TNBC and OC [17,19,40]. In our study, we

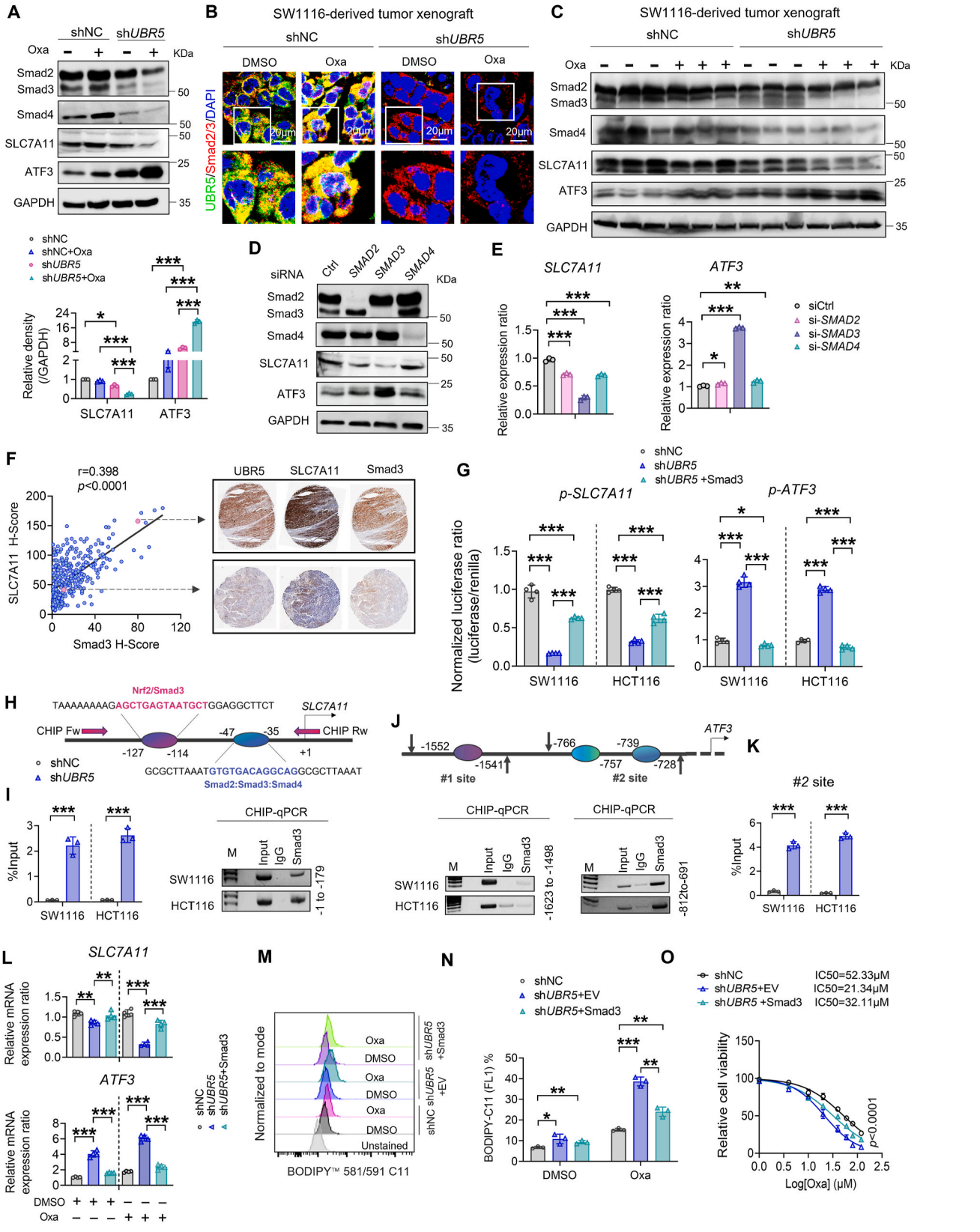

(caption on next page)

Fig 6. UBR5 regulates ATF3/SLC7A11 transcription via Smad3
A. Smad2/3/4, SLC7A11 and ATF3 protein expression in SW1116-sh*UBR5* cells with or without Oxa treatment (25 μM, 48h) was verified by western blot. The relative expression of SLC7A11 and ATF3 was quantified by normalizing to GAPDH.
B.Immunofluorescent staining of xenograft tumor sections showing reduced total & nuclear expression of Smad2/3 protein in UBR5 depleted SW1116 xenograft.
C.Smad2/3/4, SLC7A11 and ATF3 protein expression in SW1116 xenograft tumors with or without Oxa treatment was assessed by western blot.
D,E.q-PCR analysis (**E**) and western blot detection (**D**) showing SLC7A11, and ATF3 expression levels in CRC cells after Smad2, Smad3, or Smad4 silencing.
F.Representative IHC images and correlation analysis between Smad3 and SLC7A11 protein expression in human CRC TMAs (n = 329).
G.Luciferase assay of SLC7A11 promoter (left)- or ATF3 promoter (right)-driven reporters in shNC, shUBR5, and shUBR5+Smad3 CRC cells.
H–K.The Smad2/3 binding sites in the hSLC7A11 promoter region (H) or hATF3 promoter region(J) were predicted using the JASPAR and Animal TFDB3.0 websites. ChIP-PCR analysis of Smad2/3 binding at hSLC7A11 promoter (I) or hATF3 promoter (K) in SW1116 and HCT116 cells.
L.SLC7A11 and ATF3 mRNA expression in Smad3-reconstituted SW1116-shUBR5 cells was verified by qPCR.
M, N. Representative FACS images (M) and lipid ROS levels (N) in indicated SW1116 cells with or without Oxa treatment.
O.Cell viability of shNC, shUBR5, and shUBR5+Smad3 SW1116 cells treated with Oxa at indicated concentrations for 48h. The *p* value was determined by two-way ANOVA test.
Data are presented as mean ± SD. Unless otherwise noted, the *p* values were determined with unpaired two-side Student's *t*-test. $*p < 0.05$, $**p < 0.01$, $***p < 0.001$

consistently observed that UBR5 depletion enhances the cytotoxic effects of Oxa in CRC cells partially through the induction of apoptosis (Fig. 2I–M and Fig. 4H and I). However, further studies are needed to explore the molecular principles underlying this phenomenon.

A comprehensive genome-scale analysis of CRC samples indicated that TGFβ pathway remains intact and functional in the majority of CRC specimens [41]. While somatic mutations in the TGF-β1 pathway members *TGFBR2* and *SMAD4* are frequently detected in CRC, there is limited evidence for mutations affecting Smad2/3. As the central mediators of TGF-β superfamily signaling, the activities of Smad2/3 are tightly regulated to ensure that the biological effects of different ligands are exerted in a finessed manner [33,42]. In this scenario, the destruction of nuclear Smad2/3 via polyubiquitination is essential for irreversible termination of its own signaling function. Our study establishes that ubiquitination of nuclear Smad3 by UBR5 does not induce degradation via the proteasome but instead increases its protein stability. UBR5 colocalizes with Oxa-activated Smad3 in the nucleus and directly ubiquitinates it, resulting in enhanced protein expression and activity. Our findings offer new insights into the precise/stringent regulation of the TGF-β/Smad signaling pathway by a versatile proteasome system. In addition to identifying Smad3 as a new substrate for UBR5, we further defined its ubiquitination and stabilization mediated by non-canonical K11-linked polyubiquitination. The fate of ubiquitinated substrates is largely determined by distinct ubiquitin signatures, such as K11, K48, and K63 linkages. Unlike the well-characterized roles of K48- and K63-linked polyubiquitination, which primarily designate substrates for proteasomal degradation and mediate non-proteolytic signal transduction, respectively, the functions of K11-linked polyubiquitination remain less understood [43]. However, K11-linked polyubiquitin has been increasingly recognized for its role in regulating cell cycle progression, membrane trafficking, and proteasome degradation, while also paradoxically contributing to protein stabilization [44–46]. Previous studies have reported that UBR5, in conjunction with GSK-3β, enhances the stability of β-catenin by modifying it with K11- and K29-linked polyubiquitin chains in CRC cells [47]. This finding aligns with our observation that UBR5 stabilizes Smad3 through K11-linked polyubiquitination, expanding our understanding of the diverse mechanisms whereby UBR5 orchestrates various cellular signaling pathways.

It is noteworthy that the absence of UBR5 increases the sensitivity of CRC cells to Oxa treatment and renders them more vulnerable to ferroptosis induction, without a negative effect on mouse body weight. We thus propose an evidence-based promising combination strategy (UBR5 inhibition combined with RSL3) that could synergistically sensitize CRC cells to Oxa. This synergistic effect of UBR5 suppression is supported by a recent study showing that UBR5 contributes to CDK1-mediated resistance to Oxa in CRC by blocking ferroptosis via degradation of ACSL4 [48]. In addition to the transcriptional regulation of SLC7A11, we observed downregulation of genes related to ion transport and regulation in Oxa-treated SW1116-sh*UBR5* cells, based on RNA-seq analysis (Fig. 3A). Given the increasing number of UBR5-interacting proteins, which may or may not depend on its ubiquitylation activity, UBR5 may influence the expression and function of various ferroptosis-related proteins by multiple mechanisms. The efficacy and safety of a triple therapy regimen combining Oxa, ferroptosis-inducing agents, and UBR5 inhibitors warrants further investigation, not only for CRC, but also for other chemoresistant cancer types.

In summary, our study demonstrates that UBR5 promotes chemoresistance in CRC by stabilizing Smad3 through K11-linked polyubiquitination, leading to abrogated *ATF3* transcription, elevated *SLC7A11* expression, and blockade of ferroptosis. Furthermore, targeting UBR5 with a ferroptosis inducer enhances the effectiveness of Oxa-based chemotherapy against CRC. As a novel connector between chemoresistance and ferroptosis in CRC, UBR5 may hold the potential to identify the patient population that may benefit from pharmacological induction of ferroptosis. Since UBR5 dysregulation is a common feature of malignant properties in breast, ovarian and gastrointestinal cancer, UBR5-targeted strategies may have broad therapeutic applications for developing effective anticancer treatments.

4. Methods and materials

4.1. Cell culture and transfections

Human colorectal cancer (hCRC) cells (SW1116, HCT116, and SW620) and HEK293T cells were purchased from the American Type Culture Collection (ATCC, Manassas, VA, USA) in 2019 and maintained according to the instructions of the ATCC. To establish stable UBR5 knockdown cell lines, hCRC cells were transfected with the pLKO.1-sh*UBR5* plasmid using Lipofectamine 3000 as per the manufacturer's protocol and selected with puromycin antibiotic. For RNAi-mediated silencing of Smad2, Smad3, Smad4, and ATF3, SW1116-sh*UBR5* and HCT116-sh*UBR5* cells were transfected with siRNA duplexes and Lipofectamine RNAiMAX (Invitrogen, 13778075) as per the manufacturer's instructions. A nonspecific siRNA oligo (Sigma, SIC002) was used as a negative control. All targeted sequences of the siRNAs and shRNAs are summarized in Supplementary Table 3.

To generate reconstituted cell lines in CRC-sh*UBR5,* cells were transfected with pCMV-Tag2B EDD (Addgene, #37188), pCMV-Smad3-flag, and pCMV-SLC7A11-flag using Lipofectamine 3000. Stable cell lines were selected with hygromycin B and confirmed by q-PCR and western blotting. All cells were cultured at 37 °C in a humidified incubator containing 5 % CO_2. The cell lines were validated by karyotyping. All cells were routinely checked using the short tandem repeat method and tested negative for mycoplasma.

4.2. Plasmids

Full-length cDNA or fragmented DNA encoding truncated domains of Smad3 was cloned into the pCMV-flag vector. HA-Ub WT and HA-Ub mutant (K11R/K27R/K29R/K48R/K63R/K11/K29) plasmids were

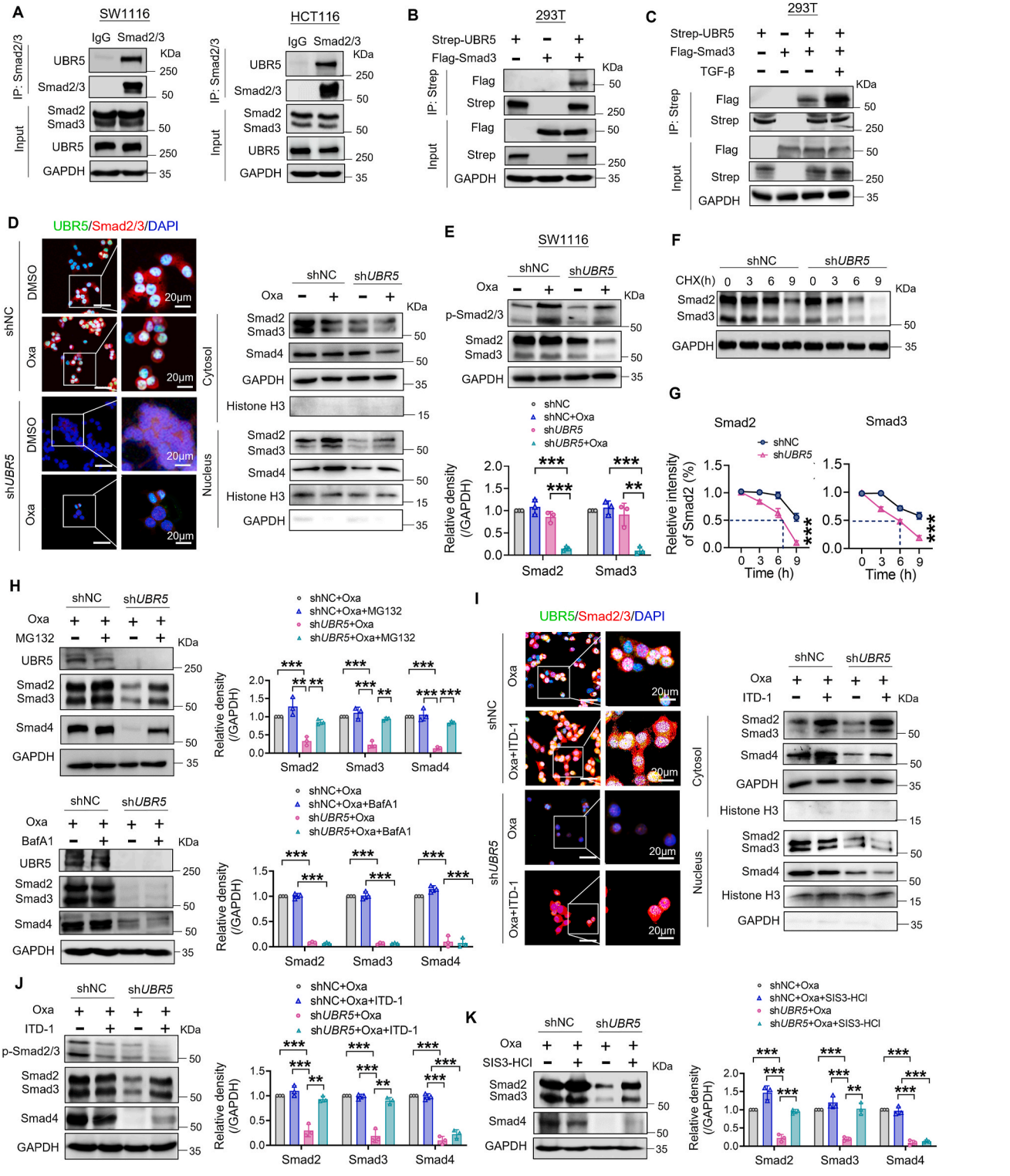

(caption on next page)

Fig 7. UBR5 enhances the protein stability of nuclear Smad2/3
A. Physical interaction of endogenous UBR5 with Smad2/3 was detected by co-IP with anti-Smad2/3 antibody in SW1116 (left) and HCT116 (right) cells.
B, C.Physical interaction of exogenous UBR5 with Smad3 was monitored by co-IP with anti-Strep antibody in HEK293T cells transfected with Strep-UBR5 or/and Flag-Smad3 expressing plasmids with or without TGF-β (2.5 μg/ml, 12h).
D.Immunofluorescent staining and western blot showing the co-localization of endogenous UBR5 with Smad2/3 and nuclear transporting of Smad2/3 in response to Oxa. All panels are of the same magnification, Scale bars:20 μm.
E.Western blot detection of the phosphorylation and total levels of Smad2/3 in SW1116 (shNC & shUBR5) cells treated with Oxa (25 μM, 48h). The relative expression of Smad2/3 was quantified by normalizing to GAPDH.
F, G.The turnover of Smad2 and Smad3 proteins in SW1116-shNC and SW1116-shUBR5 cells was measured by CHX (100 μg/ml) treatment and then detected by western blot (F) and quantified by ImageJ software (G).
H. Western blot detection of the Smad2/3, Smad4 in SW1116-shNC and SW1116-shUBR5 cells treated with vehicle, MG132 (10 μM, 8h) or BafA1 (100 nM, 24h) in the presence of Oxa (25 μM, 48h). The relative expression of Smad2/3/4 was quantified by normalizing to GAPDH.
I, J.SW1116-shNC and SW1116-shUBR5 cells were treated with vehicle, ITD-1 (10 μM, 48h) in the presence of Oxa (25 μM, 48h), and the levels of pSmad2/3, Smad2/3, and Smad4 were detected by western blot (J), the expression and cellular distribution of Smad2/3 were monitored by immunofluorescent staining and western blot (I). All panels are the same magnification. Scale bars:40 μm.
K.Western blot showing Smad2/3 and Smad4 protein expression in Oxa-treated SW1116 cells with or without SIS3HCl (10 μM, 48h). The relative expression of Smad2/3/4 was quantified by normalizing to GAPDH.
Data are presented as mean ± SD. The p value of G was determined by two-way ANOVA test. ***$p < 0.001$

obtained from MiaolingBio (Wuhan, China). Six single-site mutants of Flag-tagged Smad3 K53R, K81R, K333R, K341R, K378R, and K409R were designed for critical ubiquitination residues analysis. All mutants were generated by site-specific mutagenesis method and were confirmed by sequencing. Primers used for site-directed mutagenesis are listed in Supplementary Table 4.

4.3. Reagents

Oxa (S1224), ITD-1(S7613), RSL3(S8155), SIS3–HCl (S7959), N-acetylcysteine (S1623), BafA1(S1413), Hygromycin B (S2908) were obtained from Selleck (Houston, USA). Cycloheximide (01810), MG132 (M7449), and puromycin (P8833) were obtained from Sigma-Aldrich (Burlington, USA).

4.4. Human tissue specimens

All human tissue specimens, including TMAs containing 259 pairs of CRC and adjacent normal tissues, RNA samples from 29 matched CRC tissues and adjacent normal tissues, CRC tissues for PDX model and 66 CRC tissues with XELOX chemotherapy for IHC staining were obtained from the First Affiliated Hospital, Sun Yat-sen University with the consent of the patients, between January 2016 and December 2018. This study was approved by the Ethics Committee of the First Affiliated Hospital, Sun Yat-sen University and conducted in accordance with recognized ethical guidelines of the Declaration of Helsinki. The clinicopathological characteristics of the CRC patients whose samples were included in this study are summarized in Supplementary Tables 1 and 2

4.5. Cell viability and colony formation assay

For the cell viability assay, 1×10^4 cells were seeded into 96-well plate and treated with the indicated chemicals for 48hr. Cell viability was measured using the Cell Counting Kit-8 (MCE, HY-K0301) according to the manufacturer's instructions. For the colony forming assay, the indicated number of cells were seeded in 6-well plate and treated continuously with chemo drugs. The colonies were fixed using 4 % formaldehyde, stained with 0.05 % (w/v) crystal violet, and counted with the ImageJ v1.53c software.

4.6. RNA isolation, qRT-PCR

Total RNAs was extracted using the FastPure Cell/Tissue Total RNA Isolation Kit (Vazyme, RC112), and cDNA was synthesized using the *Evo M-MLV* RT Kit (Accurate Biology, AG11706). Quantitative PCR was performed on a QuantStudio™ 5 F (Applied Biosystem™) using the Premix Pro Taq HS qPCR Kit II (Accurate Biology, AG11702). The expression levels of the target genes were normalized with *GAPDH* abundance. The primers used for qRT-PCR are listed in Supplementary Table S5.

4.7. RNA sequencing (RNA-seq) and analysis

Total RNAs were extracted using TRIzol reagent (Invitrogen,15596026), and sequenced on Illumina Novaseq 6000 sequencing instrument (BGI, China). Differential gene analysis was performed using the DESeq package under the conditions of Fold Change ≥ 2 and adjusted p value ≤ 0.001. Using the pheatmap function on the differential gene set to draw a heatmap of differential gene clusters. According to the GO and KEGG annotation results and classifications, the differentially expressed genes were functionally classified, the phyper in R software was used for KEGG enrichment analysis, and the TermFinder package was used for GO Enrichment analysis. With a Q value of ≤ 0.05 as the threshold, candidate genes that met this condition were defined as significantly enriched.

4.8. Western blot

Cells were lysed in RIPA buffer (Beyotime, P0013B) and the lysates were centrifuged at 12,000 × rpm for 30min at 4 °C. Supernatants were collected and protein concentration was quantified by BCA protein assay kit (Beyotime, P0011). Cytoplasmic and nuclear extracts were separated from CRC cells with NE-PER™ Nuclear and Cytoplasmic Extraction Reagents (Thermo Scientific, 78833). Cell lysates were subjected to SDS-PAGE and transfected to the PVDF membrane (Merk Millipore, IPVH00010), followed by immunoblotting with the specific antibodies listed in Supplementary Table S6. The signal intensity was quantified using the Image J software.

4.9. Immunoprecipitation (IP) assay

Cells were lysed using IP lysis buffer (Beyotime, P0013) supplemented with protease inhibitor cocktail (Sigma, P8430) for 30min on ice, centrifuged and quantified with BCA protein assay kit (Beyotime, P0011). Equal amounts of cellular extracts were incubated with the primary antibodies, followed by Protein A/G PLUS-Agarose (Santa Cruz, sc-2002) on a rocker platform at 4 °C overnight. The beads were washed four times with lysis buffer and the precipitated proteins were eluted by boiling in 1 × SDS-PAGE loading buffer for 8min and then subjected to western blotting analysis. Antibodies used for IP assay are listed in Supplementary Table S6.

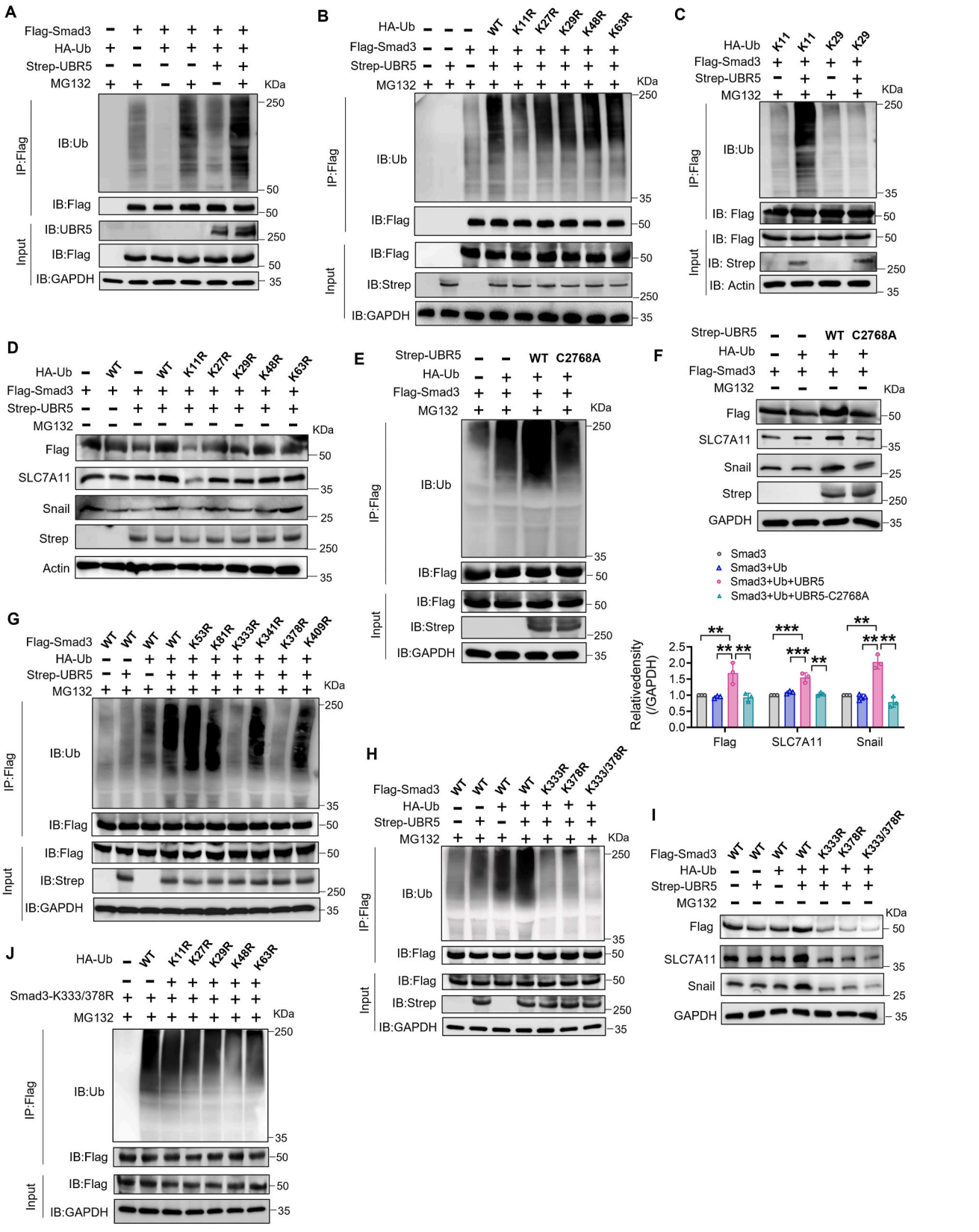

(caption on next page)

Fig 8. UBR5 stabilizes Smad3 via Lys 11-polyubiqutination at Lys^{333} and Lys^{378}.
A.Ubiquitination assay analyzed the polyubiquitination levels of Smad3 modified by exogenous UBR5 with or without MG132 (10 μM, 8h).
B, C.Ubiquitination assays with wild-type ubiquitin or ubiquitin mutants (K11R, K27R, K29R, K48R, K63R) (B); ubiquitin mutants (K11, K29) (C) analyzing the ubiquitination levels of Smad3 modified by exogenous UBR5.
D.HEK293T cells were transfected with Flag-Smad3, Strep-UBR5, and HA-ubiquitin as indicated. The expression of Flag-Smad3, SLC7A11, and Snail was detected by Western blot.
E.Ubiquitination assays with wild-type UBR5 or UBR5-C2768A analyzing the ubiquitination levels of Smad3.
F.Protein expression of Flag-Smad3, SLC7A11 and Snail in Strep-UBR5, or Strep-UBR5-C2768A overexpressed HEK293T cells.
G, H. Ubiquitination assays of WT and the mutants of Smad3 [K333R, K378R, K333/378R(H)] in HEK293T cells modified by exogenous UBR5.
I.Protein expression of Flag-Smad3 (WT, K333R, K378R, K333/378R), SLC7A11, and Snail in Strep-UBR5 overexpressed HEK293T cells.
J.Ubiquitination assays with wild-type ubiquitin or ubiquitin mutants (K11R, K27R, K29R, K48R, K63R) for Smad3 K333/378R.
Data are presented as mean ± SD. The p value of F was determined with unpaired two-side Student's t-test. $^{**}p < 0.01$, $^{***}p < 0.001$

4.10. Immunohistochemistry (IHC)

IHC assays were performed using standard methods. Briefly, paraffin-embedded sections were deparaffinized, and rehydrated. The endogenous peroxidase activity was blocked with 3 % H_2O_2 for 10min. Antigens were retrieved using sodium citrate buffer or EDTA for 10min at a sub-boiling temperature. After blocking with 10 % FBS for 1h at room temperature, the slides were incubated with primary antibody at 4 °C overnight, and then treated with secondary antibody and visualized with DAB Detection Kit (ZSGB-BIO, ZLI-9017). The nucleus was counter stained with hematoxylin. Antibodies used for IHC are listed in Supplementary Table S6.

IHC analysis was performed by two independent observers who were blinded to the results of the other makers and clinical outcomes. The images were acquired with a KF-PRO-020 scanner (Konfoong Tech). The staining intensity scored as 0 (no staining), 1+ (weak staining), 2+ (moderate staining), or 3+ (strong staining) and the extension (percentage) of expression was determined. The H-scores for tumor tissues were determined by multiplying the staining intensity and reactivity extension values (range, 0–300).

4.11. Flow cytometry analysis

Cell apoptosis was analyzed using the Annexin V-Alexa Fluor 647/PI Apoptosis Detection Kit (4A Biotech, FXP023) according to the manufacturer's instructions. In brief, culture cells were washed, dissociated, and suspended in 1 × binding buffer. Then, cells were stained with annexin V and propidium iodide (PI) at room temperature for 15 min in the dark. For cellular lipid ROS detection, cells in culture were washed and stained with 10 μM BODIPY™ 581/591C11 probe (Thermo Fisher, D3861) in the dark at 37 °C for 1hr. The cells were then disassociated and washed with PBS for three times.

For cellular ROS detection, hCRC cells were trypsinized, resuspended in PBS and incubated with 5 μM CM-H2DCF-DA probe in the dark at 37 °C for 30 min. Data acquisition was performed on the flow cytometer CytoFLEX (Beckman) and analyzed via FlowJo 10.8.1.

4.12. Immunofluorescent staining

Cells were cultured on 15 mm Glass-bottomed cell culture Dishes (Nest, 801002), fixed with 3.7 % paraformaldehyde (PFA) for 10min, permeabilized with 0.5 % Trition-X100 (in PBS) for 10 min at room temperature, followed by blocking and staining. IF staining for culture cells was performed as previously described [19]. The CM-H2DCF-DA probe (MCE, HY-D0940) was incubated at 37 °C for 30 min to visualize the cellular ROS levels. Antibodies used for immunofluorescence analysis are listed in Supplementary Table 5. Tissue apoptosis assay was performed using a Fluorometric TUNEL assay kit (Promega, G3250). Confocal microscopy images were taken under Olympus FV3000 Laser Scanning Confocal Microscope and evaluated with FV31S-SW software.

4.13. Animal experiments

Female BALB/c nude mice aged 4–6 weeks were purchased from the Laboratory Animal Center of Sun Yat-sen University (Guangzhou, China). All animal experiments were conducted in accordance with the National Institute of Health Guide for the Care and Use of Laboratory Animals. The experimental procedures were approved by the Institutional Animal Care and Use Committee of the Sun Yat-sen University (approval number: SYSU-IACUC-2022003193, SYSU-IACUC-2023355).

3.5×10^6 SW1116 tumor cells were subcutaneously injected into mice. Oxaliplatin (Selleck, S1224) monotherapy was started on day 7 post tumor inoculation, and intraperitoneal injections (7.5 mg/kg) were administered twice a week for 3 weeks. For Fer + VAD treatment, Fer (5 mg/kg) and VAD (5 mg/kg) were intraperitoneally injected into SW1116 tumor bearing mice every other day since day 7, for a total of 8 doses.

For oxaliplatin + RSL3 (Selleck, S8155) combination therapy, 5 mg/kg oxaliplatin and/or 12.5 mg/kg RSL3 were intraperitoneally or intratumorally injected into SW1116 tumor bearing mice every 3 days since day 7, for a total of 6 doses. Tumor volume was measured every 3 days since day 7 of tumor implantation and calculated using formula $V = 0.5 \times D \times W^2$ (V, volume, D, diameter, and W, width). The mice were sacrificed on day 25, and the tumors were photographed, weighed, and embedded in paraffin for further pathological analysis.

The PDX models were generated using fresh tumor samples from CRC patient that were subcutaneously implanted into the dorsal flank of mice as the first generation (F0). The patient's profile is as follows: male, 42 years, Asian, with a diagnosis of moderately differentiated rectal adenocarcinoma, pathological stage pT3N2aM0, clinical stage IIIB, microsatellite stable (MSS). Once reaching an appropriate volume, the tumors were excised, divided into equal pieces, and subcutaneously implanted into NOD/SCID mice as the second generation. 20 days post implantation, the tumor bearing mice were randomly divided into four groups. UBR5 siRNA (CAACUUAGAUCUCCUGAAA) or control siRNA (siN 0000005-4) (5 nmol per injection, RiboBio) was intratumorally injected into mice receiving Oxa (7.5 mg/kg) or PBS by i.p. injection every 3 days.

4.14. Chromatin immunoprecipitation (ChIP) assay

ChIP assays were performed using the EZ ChIP kit (Merk Millipore, 17–375) according to the manufacturer's instructions. Briefly, formaldehyde-cross linked chromatin was prepared from hCRC cells, harvested, and incubated with 5ug of anti-Smad2/3 antibody (Cell Signaling, 3102) or normal control rabbit IgG antibody. q-PCR and agarose gel electrophoresis assays were performed to detect the binding regions of the *ATF3* and *SCL7A11* promoters. Primers used for ChIP are listed in Supplementary Table S6.

4.15. Luciferase reporter assay

The h*SLC7A11*/h*ATF3* promoter regions, spanning from −2000 to +100 of exon 1 were cloned into the pGL3-Basic vector. Luciferase

activities were evaluated using the Dual-Luciferase Reporter Assay System (Promega, E1910) according to the manufacturer's instruction. hCRC cells were seeded into 12-well plate and transiently transfected with luciferase reporter plasmids plus Renilla DNA (pRL-TK) at a ratio of 10:1. Firefly luciferase activities were normalized by Renilla luciferase signal.

4.16. In vivo ubiquitination assay

HEK293T cells were transfected with HA-ubiquitin constructs together with the indicated plasmids. 10 μM proteasomal inhibitor MG132 was added 8hr before harvesting. 36hr after transfection, the cells were harvested and lysed in IP-RIPA buffer (Beyotime, P0013). Cell lysates were immunoprecipitated with anti-FLAG (Sigma, F1804) as described in the IP assay. The bound proteins were eluted by boiling in 1 × SDS-PAGE loading buffer and then subjected to western blotting analysis with indicated antibodies.

4.17. MDA and GSH assay

Subcutaneous tumors from BALB/c nude mice were lysed using lipid peroxidation Malondialdehyde (MDA) assay kit (Nanjing, A003-1) according to the manufacturer's instruction. Protein concentrations were measured with BCA protein assay kit, and the ratio of MDA to protein concentration was calculated. Cellular GSH levels were measured using GSH assay kit (Beyotime, S0053) according to the instruction, and the protein concentrations of the cell lysates were used for normalization.

4.18. Bioinformatic analysis

The data on UBR5 or SLC7A11 expression in CRC and normal tissues were extracted from the TCGA database and GEO dataset GSE39582. The survival data of CRC patients were extracted from TCGA database and GEO datasets (GSE143958, GSE14210). UBR5 expression in CRC from TCGA data was collected from the University of Alabama at Birmingham Cancer (UALCAN) data analysis portal. Based on the data of all cancer expression profiles (FPKM) of TCGA, Pearson correlations was used to calculate pairwise expression correlations between UBR5 and SLC7A11/ATF3.

4.19. Statistics and reproducibility

Statistical analysis was performed using GraphPad Prism 9 software, with a minimum of three biologically independent samples for significance. For animal experiments, each mouse was counted as a biologically independent sample. Results are presented as the mean ± SD. Comparisons between the two groups were performed using an unpaired two-sided Student's *t*-test. The survival rates were compared by the log-rank test ($p < 0.05$ was considered statistically significant). Comparison of multiple conditions was done with One-way or two-way ANOVA test. For correlation analysis, the Pearson coefficient was used.

4.20. Data and code availability

RNA-seq data that support the findings of this study have been deposited in the Gene Expression Omnibus with accession code GSE236003. All other data supporting the findings of this study are available from the corresponding authors upon reasonable request.

CRediT authorship contribution statement

Mei Song: Writing – review & editing, Writing – original draft, Supervision, Project administration, Methodology, Funding acquisition, Data curation, Conceptualization. **Shuting Huang:** Formal analysis, Data curation. **Xiaoxue Wu:** Formal analysis, Data curation. **Ziyi Zhao:** Formal analysis, Data curation. **Xiaoting Liu:** Formal analysis, Data curation. **Chong Wu:** Formal analysis, Data curation. **Mengru Wang:** Data curation. **Jialing Gao:** Data curation. **Zunfu Ke:** Resources, Funding acquisition. **Xiaojing Ma:** Writing – review & editing, Conceptualization. **Weiling He:** Supervision, Investigation, Funding acquisition.

Declaration of competing interest

The authors declare no competing interests.

Data availability

Data will be made available on request.

Acknowledgements

We thank Yunfei. Li (Southern University of Science and Technology) for kindly gifting the YF101-Strep-UBR5, and YF101-Strep-UBR5-C2768A plasmids. This work was supported in part by the National Natural Science Foundation of China (82303923, 92359302,82330065), National Key Research And Development Plan (2022YFC3401000), Guangdong Basic and Applied Basic Research Foundation (2024A1515013156, 2021B1515230009), Guangdong Provincial Key Areas R&D Programs of "Precision medicine and stem cells" (2023B1111020005), the Natural Science Foundation for Outstanding Youth Team Project of Guangdong Province (2024B1515040030), Guangzhou or Guangdong Science and Technology Planning Program (2023B1111020005, 2023B03J0106).

Appendix A. Supplementary data

Supplementary data to this article can be found online at https://doi.org/10.1016/j.redox.2024.103349.

References

[1] R.L. Siegel, K.D. Miller, A. Fuchs Hejemal, Cancer statistics, 2022, Ca - Cancer J. Clin. 72 (2022) 7–33, https://doi.org/10.3322/caac.21708.
[2] M.L. Rothenberg, Efficacy of oxaliplatin in the treatment of colorectal cancer, Oncology 14 (9–14 12 Suppl 11) (2000).
[3] C. Bockelman, B.E. Engelmann, T. Kaprio, B. Hansen Tfglimelius, Risk of recurrence in patients with colon cancer stage II and III: a systematic review and meta-analysis of recent literature, Acta Oncol. 54 (2015) 5–16, https://doi.org/10.3109/0284186X.2014.975839.
[4] E. Auclin, A. Zaanan, D. Vernerey, R. Douard, C. Gallois, P. Laurent-Puig, et al., Subgroups and prognostication in stage III colon cancer: future perspectives for adjuvant therapy, Ann. Oncol. 28 (2017) 958–968, https://doi.org/10.1093/annonc/mdx030.
[5] R. Yang, B. Yi Mxiang, Novel insights on lipid metabolism alterations in drug resistance in cancer, Front. Cell Dev. Biol. 10 (2022) 875318, https://doi.org/10.3389/fcell.2022.875318.
[6] Y.G. Assaraf, A. Brozovic, A.C. Goncalves, D. Jurkovicova, A. Line, M. Machuqueiro, et al., The multi-factorial nature of clinical multidrug resistance in cancer, Drug Resist. Updates 46 (2019) 100645, https://doi.org/10.1016/j.drup.2019.100645.
[7] J. Guo, B. Xu, Q. Han, H. Zhou, Y. Xia, C. Gong, et al., Ferroptosis: a novel anti-tumor action for cisplatin, Cancer Res Treat 50 (2018) 445–460, https://doi.org/10.4143/crt.2016.572.
[8] J.P. Friedmann Angeli, M. Krysko Dvconrad, Ferroptosis at the crossroads of cancer-acquired drug resistance and immune evasion, Nat. Rev. Cancer 19 (2019) 405–414, https://doi.org/10.1038/s41568-019-0149-1.
[9] C. Zhang, X. Liu, S. Jin, R. Chen Yguo, Ferroptosis in cancer therapy: a novel approach to reversing drug resistance, Mol. Cancer 21 (2022) 47, https://doi.org/10.1186/s12943-022-01530-y.
[10] B.R. Stockwell, J.P. Friedmann Angeli, H. Bayir, A.I. Bush, M. Conrad, S.J. Dixon, et al., Ferroptosis: a regulated cell death nexus linking metabolism, redox Biology, and disease, Cell 171 (2017) 273–285, https://doi.org/10.1016/j.cell.2017.09.021.
[11] N. Jyotsana, K.E. Ta KtdelGiorno, The role of cystine/glutamate antiporter slc7a11/xCT in the pathophysiology of cancer, Front. Oncol. 12 (2022) 858462 doi./10.3389/fonc.2022.858462.
[12] X. Xu, X. Zhang, C. Wei, D. Zheng, X. Lu, Y. Yang, et al., Targeting SLC7A11 specifically suppresses the progression of colorectal cancer stem cells via inducing ferroptosis, Eur. J. Pharmaceut. Sci. 152 (2020) 105450, https://doi.org/10.1016/j.ejps.2020.105450.

[13] H.Q. Ju, Y.X. Lu, D.L. Chen, T. Tian, H.Y. Mo, X.L. Wei, et al., Redox regulation of stem-like cells though the CD44v-xCT Axis in colorectal cancer: mechanisms and therapeutic implications, Theranostics 6 (2016) 1160–1175, https://doi.org/10.7150/thno.14848.
[14] M.Z. Ma, G. Chen, P. Wang, W.H. Lu, C.F. Zhu, M. Song, et al., Xc- inhibitor sulfasalazine sensitizes colorectal cancer to cisplatin by a GSH-dependent mechanism, Cancer Lett. 368 (2015) 88–96, https://doi.org/10.1016/j.canlet.2015.07.031.
[15] D.N. Saunders, S.L. Hird, S.L. Withington, S.L. Dunwoodie, M.J. Henderson, C. Biben, et al., Edd, the murine hyperplastic disc gene, is essential for yolk sac vascularization and chorioallantoic fusion, Mol. Cell Biol. 24 (2004) 7225–7234, https://doi.org/10.1128/MCB.24.16.7225-7234.2004.
[16] E. Kinsella, N. Dora, D. Mellis, L. Lettice, P. Deveney, R. Hill, et al., Use of a conditional Ubr5 mutant allele to investigate the role of an N-end rule ubiquitin-protein ligase in hedgehog signalling and embryonic limb development, PLoS One 11 (2016) e0157079, https://doi.org/10.1371/journal.pone.0157079.
[17] L. Liao, M. Song, X. Li, L. Tang, T. Zhang, L. Zhang, et al., E3 ubiquitin ligase UBR5 drives the growth and metastasis of triple-negative breast cancer, Cancer Res. 77 (2017) 2090–2101, https://doi.org/10.1158/0008-5472.CAN-16-2409.
[18] M. Song, C. Wang, H. Wang, T. Zhang, J. Li, R. Benezra, et al., Targeting ubiquitin protein ligase E3 component N-recognin 5 in cancer cells induces a CD8+ T cell mediated immune response, OncoImmunology 9 (2020) 1746148, https://doi.org/10.1080/2162402X.2020.1746148.
[19] M. Song, O.O. Yeku, S. Rafiq, T. Purdon, X. Dong, L. Zhu, et al., Tumor derived UBR5 promotes ovarian cancer growth and metastasis through inducing immunosuppressive macrophages, Nat. Commun. 11 (2020) 6298, https://doi.org/10.1038/s41467-020-20140-0.
[20] J. Wang, X. Zhao, L. Jin, Y. Wu Gyang, UBR5 contributes to colorectal cancer progression by destabilizing the tumor suppressor ECRG4, Dig. Dis. Sci. 62 (2017) 2781–2789, https://doi.org/10.1007/s10620-017-4732-6.
[21] L. Chen, R. Yuan, C. Wen, T. Liu, Q. Feng, X. Deng, et al., E3 ubiquitin ligase UBR5 promotes pancreatic cancer growth and aerobic glycolysis by downregulating FBP1 via destabilization of C/EBPalpha, Oncogene 40 (2021) 262–276, https://doi.org/10.1038/s41388-020-01527-1.
[22] B. Wu, M. Song, Q. Dong, G. Xiang, J. Li, X. Ma, et al., UBR5 promotes tumor immune evasion through enhancing IFN-gamma-induced PDL1 transcription in triple negative breast cancer, Theranostics 12 (2022) 5086–5102, https://doi.org/10.7150/thno.74989.
[23] M.J. Henderson, A.J. Russell, S. Hird, M. Munoz, J.L. Clancy, G.M. Lehrbach, et al., EDD, the human hyperplastic discs protein, has a role in progesterone receptor coactivation and potential involvement in DNA damage response, J. Biol. Chem. 277 (2002) 26468–26478, https://doi.org/10.1074/jbc.M203527200.
[24] A. Sanchez, A. De Vivo, N. Uprety, J. Kim, S.M. Stevens Jr., Y. Kee, BMI1-UBR5 axis regulates transcriptional repression at damaged chromatin, Proc. Natl. Acad. Sci. U.S.A. 113 (2016) 11243–11248, https://doi.org/10.1073/pnas.1610735113.
[25] X. Qiao, Y. Liu, M.L. Prada, A.K. Mohan, A. Gupta, A. Jaiswal, et al., UBR5 is coamplified with MYC in breast tumors and encodes an ubiquitin ligase that limits MYC-dependent apoptosis, Cancer Res. 80 (2020) 1414–1427, https://doi.org/10.1158/0008-5472.CAN-19-1647.
[26] Y. Yang, J. Zhao, Y. Mao, G. Lin, Z. Li Fjiang, UBR5 over-expression contributes to poor prognosis and tamoxifen resistance of ERa+ breast cancer by stabilizing beta-catenin, Breast Cancer Res. Treat. 184 (2020) 699–710, https://doi.org/10.1007/s10549-020-05899-6.
[27] A. Bradley, H. Zheng, A. Ziebarth, W. Sakati, M. Branham-O'Connor, J.B. Blumer, et al., EDD enhances cell survival and cisplatin resistance and is a therapeutic target for epithelial ovarian cancer, Carcinogenesis 35 (2014) 1100–1109, https://doi.org/10.1093/carcin/bgt489.
[28] H. Kalkavan, S. Ruhl, D.R. Shaw Jjpgreen, Non-lethal outcomes of engaging regulated cell death pathways in cancer, Nat. Can. (Ott.) 4 (2023) 795–806, https://doi.org/10.1038/s43018-023-00571-6.
[29] JConrad M. Zheng, The metabolic underpinnings of ferroptosis, Cell Metabol. 32 (2020) 920–937, https://doi.org/10.1016/j.cmet.2020.10.011.
[30] P. Koppula, B. Zhuang Lgan, Cystine transporter SLC7A11/xCT in cancer: ferroptosis, nutrient dependency, and cancer therapy, Protein Cell 12 (2021) 599–620, https://doi.org/10.1007/s13238-020-00789-5.
[31] L. Wang, Y. Liu, T. Du, H. Yang, L. Lei, M. Guo, et al., ATF3 promotes erastin-induced ferroptosis by suppressing system Xc(.), Cell Death Differ. 27 (2020) 662–675, https://doi.org/10.1038/s41418-019-0380-z.
[32] R.F. Shearer, M. Iconomou, D.N. Watts Cksaunders, Functional roles of the E3 ubiquitin ligase UBR5 in cancer, Mol. Cancer Res. 13 (2015) 1523–1532, https://doi.org/10.1158/1541-7786.MCR-15-0383.
[33] Y. Zhang, C. Chang, D.J. Gehling, R. Hemmati-Brivanlou Aderynck, Regulation of Smad degradation and activity by Smurf2, an E3 ubiquitin ligase, Proc. Natl. Acad. Sci. U.S.A. 98 (2001) 974–979, https://doi.org/10.1073/pnas.98.3.974.
[34] D.H. Kim, W.D. Kim, S.K. Kim, S.J. Moon Dhlee, TGF-beta1-mediated repression of SLC7A11 drives vulnerability to GPX4 inhibition in hepatocellular carcinoma cells, Cell Death Dis. 11 (2020) 406, https://doi.org/10.1038/s41419-020-2618-6.
[35] A.C. Mullen, D.A. Orlando, J.J. Newman, J. Loven, R.M. Kumar, S. Bilodeau, et al., Master transcription factors determine cell-type-specific responses to TGF-beta signaling, Cell 147 (2011) 565–576, https://doi.org/10.1016/j.cell.2011.08.050.
[36] M. Morikawa, D. Koinuma, C.H. Miyazono Kheldin, Genome-wide mechanisms of Smad binding, Oncogene 32 (2013) 1609–1615, https://doi.org/10.1038/onc.2012.191.
[37] K. Isogaya, D. Koinuma, S. Tsutsumi, R.A. Saito, K. Miyazawa, H. Aburatani, et al., A Smad3 and TTF-1/NKX2-1 complex regulates Smad4-independent gene expression, Cell Res. 24 (2014) 994–1008, https://doi.org/10.1038/cr.2014.97.
[38] N. Dompe, C.S. Rivers, L. Li, S. Cordes, M. Schwickart, E.A. Punnoose, et al., A whole-genome RNAi screen identifies an 8q22 gene cluster that inhibits death receptor-mediated apoptosis, Proc. Natl. Acad. Sci. U.S.A. 108 (2011) E943–E951, https://doi.org/10.1073/pnas.1100132108.
[39] K. Matsuura, N.J. Huang, K. Cocce, S. Zhang Lkornbluth, Downregulation of the proapoptotic protein MOAP-1 by the UBR5 ubiquitin ligase and its role in ovarian cancer resistance to cisplatin, Oncogene 36 (2017) 1698–1706, https://doi.org/10.1038/onc.2016.336.
[40] Z. Yu, X. Dong, M. Song, A. Xu, Q. He, H. Li, et al., Targeting UBR5 inhibits postsurgical breast cancer lung metastases by inducing CDC73 and p53 mediated apoptosis, Int. J. Cancer 154 (2024) 723–737, https://doi.org/10.1002/ijc.34769.
[41] N. Cancer Genome Atlas, Comprehensive molecular characterization of human colon and rectal cancer, Nature 487 (2012) 330–337, https://doi.org/10.1038/nature11252.
[42] J. Lo Rsmassague, Ubiquitin-dependent degradation of TGF-beta-activated smad2, Nat. Cell Biol. 1 (1999) 472–478, https://doi.org/10.1038/70258.
[43] W. Tracz Mbialek, Beyond K48 and K63: non-canonical protein ubiquitination, Cell. Mol. Biol. Lett. 26 (2021) 1, https://doi.org/10.1186/s11658-020-00245-6.
[44] J. Zinngrebe, A. Montinaro, H. Peltzer Nwalczak, Ubiquitin in the immune system, EMBO Rep. 15 (2014) 28–45, https://doi.org/10.1002/embr.201338025.
[45] Z. Li, Y. Wang, Y. Li, W. Yin, L. Mo, X. Qian, et al., Ube2s stabilizes beta-Catenin through K11-linked polyubiquitination to promote mesendoderm specification and colorectal cancer development, Cell Death Dis. 9 (2018) 456, https://doi.org/10.1038/s41419-018-0451-y.
[46] J. Wang, Y. Zhang, J. Hou, X. Qian, H. Zhang, Z. Zhang, et al., Ube2s regulates Sox 2 stability and mouse ES cell maintenance, Cell Death Differ. 23 (2016) 393–404, https://doi.org/10.1038/cdd.2015.106.
[47] A. Hay-Koren, M. Caspi, R. Zilberberg Arosin-Arbesfeld, The EDD E3 ubiquitin ligase ubiquitinates and up-regulates beta-catenin, Mol. Biol. Cell 22 (2011) 399–411, https://doi.org/10.1091/mbc.E10-05-0440.
[48] K. Zeng, W. Li, Y. Wang, Z. Zhang, L. Zhang, W. Zhang, et al., Inhibition of CDK1 overcomes oxaliplatin resistance by regulating ACSL4-mediated ferroptosis in colorectal cancer, Adv. Sci. 10 (2023) e2301088, https://doi.org/10.1002/advs.202301088.